INTERNATIONAL CENTER FOR NUMERICAL METHODS IN ENGINEERING

Finite Element Procedures for Incompressible and Compressible Flows

E. Oñate
F. Quintana
R. Codina
J. Miquel

Publication, CIMNE Nº 14, October 1991

Finite Element Procedures for Incompressible and Compressible Flows

E. Oñate
F. Quintana
R. Codina
J. Miquel

Publication CIMNE Nº-14, October 1991

International Center for Numerical Methods in Engineering
Gran Capitán s/n, 08034 Barcelona, Spain

INDEX

1. INTRODUCTION

This papers summarizes the research carried out at the International Center for Numerical Methods in Engineering of Barcelona (CIMNE) up to September 1991 in the development of finite element methods for the solution of incompressible and compressible flows. The main motivations for this research have been the need for efficient numerical methods for the solution of non–Newtonian incompressible creeping flows typical of metal forming applications, and the modelling of high speed compressible flows in aeronautic and aerospace problems.

The research developed can be classified into the following topics:

a) Development of compatible finite elements for solution of incompressible and compressible inviscid and viscous flows under high speed conditions. The finite elements algorithms developed have been based in both Stream–Line–Petrov-Galerkin (SUPG) and Taylor-Galerkin methods. Non structured grid refinement techniques have also been used. Particular emphasis has been put in the study of the stability of the solution, and, in particular in the vicinities of the stagnation point.

b) Development of adequate error estimators and a mesh generator for combined structured/non structured meshes for the adaptive grid analysis of Navier-Stokes flows with particular emphasis in the problems associated to the boundary layer.

c) Verification of the efficiency and accuracy of the methodologies and algorithms developed for different 2D incompressible and compressible flows for inviscid and viscous situations.

In the following pages we present an overview of the algorithms and methods developed. The lay out of the report is as follows. First incompressible flows are dealt with. Here the basis of the SUPG approach for the mixed velocity-pressure and penalty formulations is described together with the methodology followed to derive compatible finite elements satisfying the LBB condition. Some techniques for pressure recovery, circumvection of the LBB restriction and extension of the finite element formulation to a finite volume format are also discussed.

The second part of the report deals with compressible flows. Here a brief description of both Petrov-Galerkin and Taylor-Galerkin approaches developed are described for both inviscid and viscous situations.

The third part of the report is devoted to the methods for error estimation, mesh generation, and adaptive grid refinement using non-structured finite element meshes. The use of a combination of a structured mesh for modelling the boundary layer zone and a non-structured mesh for the rest of the domain is also briefly described.

In the last part of the report some examples of application of the methods developed to incompressible and compressible 2D flow situations are presented.

The examples include 2D incompressible flow past a ramp and a cylinder. Mach 5 compressible insvicid flow over a compression corner and also for a compression/expansion problem. Mach 3 compressible inviscid flow over a 2D vedge, Mach 10 compressible viscous flow over a 2D ramp and Mach 8.5 compressible inviscid and viscous flows past a double ellipse. Finally some conclusions of the research performed are presented.

2. FINITE ELEMENT ANALYSIS OF INCOMPRESSIBLE FLOW

2.1 Basic equations

Table I summarizes the basic equations of incompressible viscous flow [37]. In the table $\mathbf{u}$, $\dot{\boldsymbol{\varepsilon}}$ and $\boldsymbol{\sigma}$ are the velocity, strain rate and stress vectors, respectively; p is the fluid pressure, $\mathbf{b}_0$ the vector of forces per unit volume (area), ρ the density and μ the viscosity. The energy balancing equation will be neglected here for simplicity.

Note that substituting the strain rate-velocity and stress–strain rate equations into the momentum equation, the usual form of the Navier-Stokes equations is found. The two basic equations of the problem (momentum and incompressibility) can therefore be written in terms of the velocities as

$$\rho\left[\frac{\partial \mathbf{u}}{\partial t}+(\nabla \mathbf{u}^T)^T\mathbf{u}\right]-\mathbf{L}^T\mathbf{D}\mathbf{L}\mathbf{u}+\mathbf{L}^T\mathbf{m}p-\mathbf{b}_0=\mathbf{0} \tag{1a}$$

$$\dot{\varepsilon}_{ii}\equiv\nabla^T\mathbf{u}=0 \tag{1b}$$

The finite element solution of eqs.(1) can be attempted in many different ways via a mixed velocity-pressure ($\mathbf{u}-p$) formulation [30], [37]; a penalty formulation [34], [37]; a least square formulation [13], [27]; an augmented Lagrangian formulation [7]; a mixed velocity-pressure-deviatoric strain formulation [30], [37]; a stream line formulation [37], etc. In our research we have considered only the $\mathbf{u}-p$ and penalty formulations in the context of a Strem-Line Petrov-Galerkin (SUPG) approach.

2.2 A SUPG velocity-pressure finite element formulation

We will consider the standard SUPG weighted integral form of eqs.(1) as [2']

$$\int_\Omega \hat{\mathbf{W}}_u^T\left[\rho\left(\frac{\partial \mathbf{u}}{\partial t}+(\nabla \mathbf{u}^T)^T\mathbf{u}\right)-\mathbf{L}^T\mathbf{D}\mathbf{L}\mathbf{u}+\mathbf{L}^T\mathbf{m}p-\mathbf{b}_0\right]d\Omega=0 \tag{2a}$$

$$\int_\Omega W_p\nabla^T\mathbf{u}d\Omega=0 \tag{2b}$$

The SUPG weighthing functions to be considered for the momentum equation are of the form

Equilibrium (momentum)

$$\mathbf{L}^T\boldsymbol{\sigma} + \mathbf{b}_0 - \rho\left(\frac{\partial \mathbf{u}}{\partial t} + (\nabla \mathbf{u}^T)^T\mathbf{u}\right) = 0$$

Strain rate-velocity

$$\dot{\boldsymbol{\varepsilon}} = \mathbf{L}\mathbf{u}$$

Stress-strain rate

$$\boldsymbol{\sigma} = \mathbf{D}\dot{\boldsymbol{\varepsilon}} - \mathbf{m}p \quad ; \quad p = -\frac{\sigma_{ii}}{3}$$

Incompressibility

$$\dot{\varepsilon}_{ii} \equiv \nabla^T\mathbf{u} = \mathbf{m}^T\mathbf{L}\mathbf{u} = 0$$

2D flow:

$$\mathbf{u} = [u, v]^T \quad , \quad \dot{\boldsymbol{\varepsilon}} = [\dot{\varepsilon}_x, \dot{\varepsilon}_x, \dot{\gamma}_{xy}]^T \quad , \quad \boldsymbol{\sigma} = [\sigma_x, \sigma_y, \tau_{xy}]^T$$

$$m = [1,1,0]^T \quad , \quad \mathbf{L} = \begin{bmatrix} \frac{\partial}{\partial x} & 0 \\ 0 & \frac{\partial}{\partial y} \\ \frac{\partial}{\partial y} & \frac{\partial}{\partial x} \end{bmatrix} \quad , \quad \mathbf{D} = \mu \begin{bmatrix} 2 & 0 & 0 \\ 0 & 2 & 0 \\ 0 & 0 & 1 \end{bmatrix}$$

$$\mathbf{b}_0 = [b_{0x}, b_{0y}]^T \quad , \quad \nabla = [\frac{\partial}{\partial x}, \frac{\partial}{\partial y}]^T$$

Table I. Basic equations of incompressible fluid flow.

$$\hat{\mathbf{W}}_u = \mathbf{W}_u + \bar{\mathbf{W}}_u \tag{3}$$

where $\mathbf{W}_u$ is continuous across interelement boundaries and $\bar{\mathbf{W}}_u$ is the discontinous stream upwind contribution. For the continuity equations both continuous and discontinuos W_p functions can be used. Each of $\mathbf{W}_u$, $\bar{\mathbf{W}}_u$ and W_p are assumed to be smooth on element interious. For convenience the viscosity and pressure terms in (2a) are integrated by parts to give

$$\int_\Omega \mathbf{W}_u^T \rho \left[\frac{\partial \mathbf{u}}{\partial t} + (\nabla \mathbf{u}^T)^T \mathbf{u}^T \right] d\Omega + \int_\Omega \left[(\mathbf{L}\mathbf{W}_u)^T \mathbf{D}\mathbf{L}\mathbf{u} - (\mathbf{L}\mathbf{W}_u)^T \mathbf{m}p \right] d\Omega =$$
$$= \int_\Omega \mathbf{W}_u^T \mathbf{b}_0 d\Omega + \oint_\Gamma \mathbf{W}_u^T \mathbf{t} d\Gamma + \bar{\mathbf{r}} \qquad (4)$$

where $\mathbf{t}$ are the tractions acting on the fluid boundary Γ. The term $\bar{\mathbf{r}}$ takes into account the use of discontinuous weighting functions in the SUPG approach and it can be generically written as

$$\bar{\mathbf{r}} = -\sum_{e=1}^{NE} \int_{\Omega^{(e)}} \bar{\mathbf{W}}_u^T \left[\rho \frac{\partial \mathbf{u}}{\partial t} + \rho (\nabla \mathbf{u}^T)^T \mathbf{u} - \mathbf{L}^T \boldsymbol{\sigma} - \mathbf{b}_0 \right] d\Omega \qquad (5)$$

where NE is the total number of elements.

A standard finite element discretization can now be chosen in which velocities and pressure are independently interpolated using different shape (basis) functions $\mathbf{N}_u$ and $\mathbf{N}_p$ as

$$\mathbf{u} = \mathbf{N}_u \bar{\mathbf{u}} \quad , \quad p = \mathbf{N}_p \bar{\mathbf{p}} \qquad (6)$$

where $\bar{\mathbf{u}}$ and $\bar{\mathbf{p}}$ stand for the nodal velocity and pressure variables. Substitution of (6) into (5) and (4) yields the following system of discretized equations

$$\boxed{\mathbf{M}\dot{\mathbf{a}} + \mathbf{f}_a + \mathbf{f} = 0} \qquad (7a)$$

where

$$\mathbf{M} = \begin{bmatrix} \bar{\mathbf{M}} & \mathbf{0} \\ \mathbf{0} & \mathbf{0} \end{bmatrix} \quad ; \quad \mathbf{f}_a = \begin{bmatrix} \mathbf{K} + \bar{\mathbf{K}} & \mathbf{K}^p \\ \bar{\mathbf{K}}^p & \mathbf{0} \end{bmatrix} \mathbf{a}$$
$$\mathbf{f} = \begin{Bmatrix} \bar{\mathbf{f}} \\ \mathbf{0} \end{Bmatrix} \quad , \quad \mathbf{a} = \begin{Bmatrix} \bar{\mathbf{u}} \\ \bar{\mathbf{p}} \end{Bmatrix} \qquad (7b)$$

The form of the different matrices appearing in (7b) for an individual element can be seen in Table II. The global system (7a) can be assembled from the element contributions in the standard form.

Note that the discontinuous SUPG weighting introduces the computation of second derivative terms in $\mathbf{K}_{ij}^{(e)}$. Also in this case the system of equations (7b) is clearly non symmetric.

For stationary flow conditions ($\frac{\partial \mathbf{a}}{\partial t} = 0$) and system (7a) reduces to

$$\begin{bmatrix} \mathbf{K} + \bar{\mathbf{K}} & \mathbf{K}^p \\ \bar{\mathbf{K}}^p & \mathbf{0} \end{bmatrix} \begin{Bmatrix} \bar{\mathbf{u}} \\ \bar{\mathbf{p}} \end{Bmatrix} = \begin{Bmatrix} \bar{\mathbf{f}} \\ \mathbf{0} \end{Bmatrix} \qquad (8)$$

$$\mathbf{K}_{ij}^{(e)} = \int_{\Omega^{(e)}} [\bar{\mathbf{B}}_i^T \mathbf{D} \mathbf{B}_j + [\bar{\mathbf{W}}_{u_i}^T] \mathbf{L}^T \mathbf{D} \mathbf{B}_j] d\Omega \quad ; \quad \bar{\mathbf{K}}_{ij}^{(e)} = \int_{\Omega^{(e)}} \rho [\hat{\mathbf{W}}_{u_i}]^T [\nabla (\mathbf{N}_u \bar{\mathbf{u}})^T]^T \mathbf{N}_{u_j} d\Omega$$

$$[\mathbf{K}_{ij}^{p}]^{(e)} = -\int_{\Omega^{(e)}} [\bar{\mathbf{B}}_i^T \mathbf{m} N_{p_j} - [\bar{\mathbf{W}}_{u_i}]^T \mathbf{L}^T \mathbf{m} N_{p_j}] d\Omega \quad ; \quad \bar{\mathbf{M}}_{ij}^{(e)} = \int_{\Omega^{(e)}} [\hat{\mathbf{W}}_{u_i}]^T \rho \mathbf{N}_{u_j} d\Omega$$

$$[\bar{\mathbf{K}}_{ij}^{p}]^{(e)} = -\int_{\Omega} W_{p_i} \mathbf{m} \mathbf{B}_j d\Omega \quad ; \quad \bar{\mathbf{f}}_i^{(e)} = \int_{\Omega^{(e)}} [\mathbf{W}_{u_i}]^T \mathbf{b}_0 d\Omega + \oint_{\Gamma^{(e)}} [\mathbf{W}_{u_i}]^T \mathbf{t} d\Gamma$$

with $\mathbf{B}_i = \mathbf{L} \mathbf{N}_{u_i}$, $\bar{\mathbf{B}}_i = \mathbf{L} \mathbf{W}_{u_i}$

Table II. Different element matrices and vectors involved in the SUPG velocity-pressure formulation.

For slow flow conditions the convective acceleration terms can be neglected and therefore matrix $\bar{\mathbf{K}} = 0$ in eqs.(7b) and (9). The resulting form has been widely used in past years for creeping flow problems [33, 34]. Note that in this case the equations are analogous to that of incompressible elasticity, which provides an interesting unified framework for solving Stokes fluid and solid problems [30,33,37].

It is well known [31,35] that system (8) has solution if and only if

$$n_u \geq n_p \tag{9}$$

where n_u and n_p are the number of effective velocity and pressure nodal variables in the finite element mesh (after discounting prescribed values).

Eq.(9) is a *necessary* condition to be satisfied for the velocity and pressure interpolations chosen. More generally, the velocity and pressure fields must satisfy the well-known LBB div-stability condition [2], [14], [37]. Figure 1 shows some of the possibilities for triangular and quadrilateral elements explored in this research. It can be seen that some of the simpler options like the triangular element with a linear approximation for both velocities and pressures fail to satisfy eq.(9) and therefore is not, in principle, adequate for incompressible flow problems [1]. More options of admisible elements satisfying (9) and the LBB condition can be found in [37].

2.3 Choice of weighting functions $\hat{\mathbf{W}}_u$ and W_p

The most obvious choice for $\hat{\mathbf{W}}_u$ and W_p is the Galerkin one with $\hat{\mathbf{W}}_u = \mathbf{N}_u$ and $W_p = N_p$. This leads to a symmetric system of equations as can be easily checked from Table II.

However, it is well known that Galerkin weighting is not optimal for convection/diffussion type problems. Moreover, it leads to instabilities in the numerical solution for high values of the Peclet number. The reasons of this are well known and have been widely reported in literature [4,5,10,12,15,37].

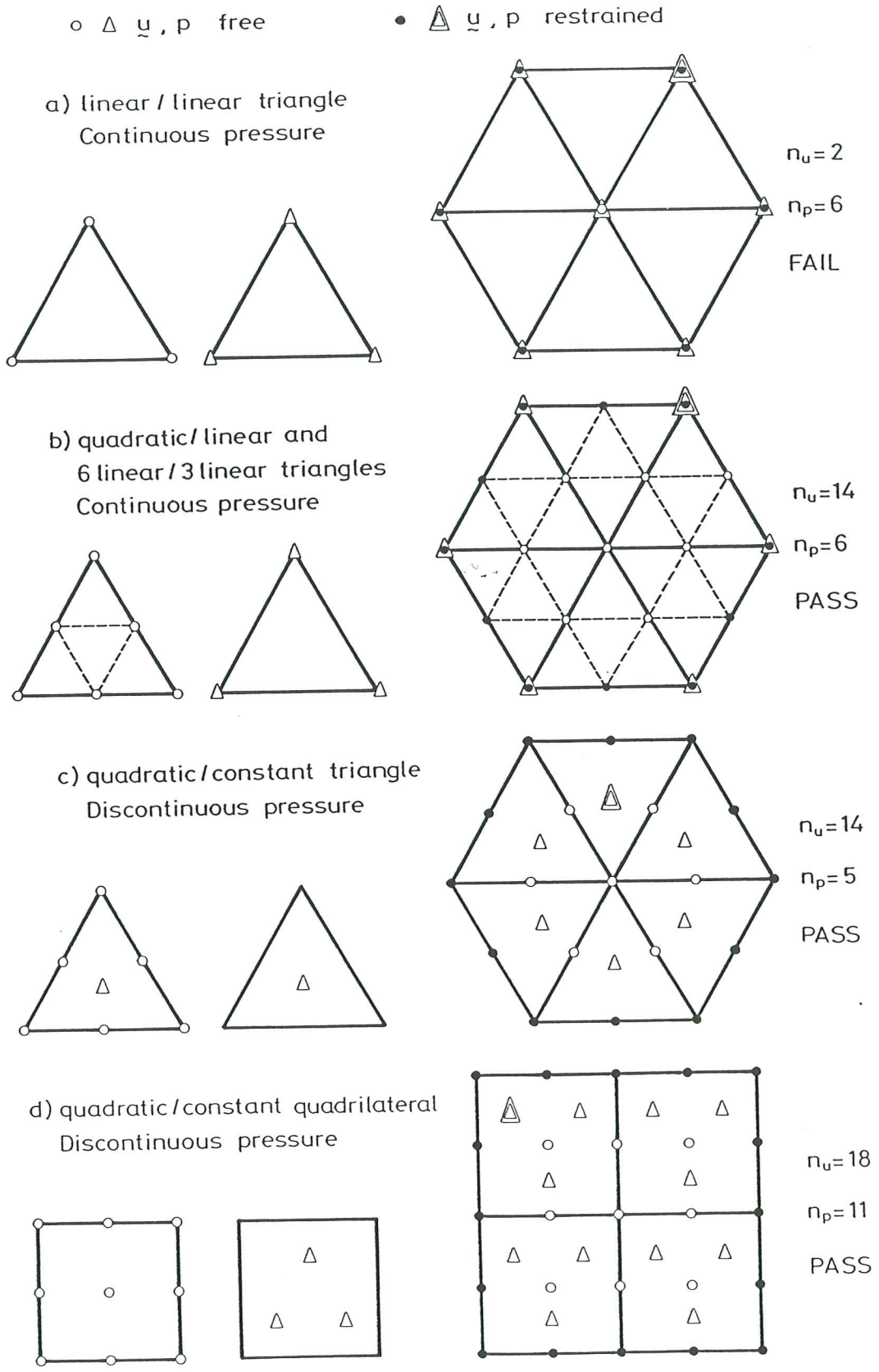

Figure 1 Some triangular and quadrilateral elements with velocity [O] and pressure [Δ] interpolations.

These problems can be overcome by the use of SUPG weighting with [2']

$$\mathbf{W}_u = \mathbf{N}_u + \frac{\alpha^{(e)} h^{(e)}}{2\|\mathbf{u}\|} \mathbf{u}^T \nabla \mathbf{N}_u \tag{10a}$$

$$W_p = N_p \tag{10b}$$

In (10a) $h^{(e)}$ is a measure of the element size and $\alpha^{(e)}$ is a parameter which is a function of the velocity, the element size and the physical parameters of the flow (viscosity, density, etc.). For 1D convection/diffusion problems an optimal value of α can be found giving the exact solution at the nodes. Extension to 2D/3D problems are based in the 1D values with some modifications regarding the definition of the "element size" $h^{(e)}$ and appropiate weighting along the flux direction. Figures 2 and 3 gives the values of $\alpha^{(e)}$ for some 1D and 2D elements. For further discussion the reader is addresed to [4,5,10,12,15,37].

It is also welll known that Petrov-Galerkin weighting has a simple interpretation for steady state homogeneous problems solved with linear finite elements as it is then equivalent to the addition of an artificial balancing diffusion in the direction of the flow. The same interpretation does not hold exactly if flow sources are present or higher order finite element interpolations are used. Nevertheless, Petrov-Galerkin weighting can always be associated to the addition of some kind of balancing diffussion which value can not however always be precisely defined. Another interpretation of Petrov-Galerkin weighting comes from the analogy with "upwinding" methods widely used in finite difference schemes. This analogy has allowed to obtain alternative expressions to the form (10a) [4], [10], [12].

The SUPG $\mathbf{u}/p$ formulation provides an adequate framework for deriving "robust" compatible finite element approximations. Hovewer, the practical application of the formulation is somehow cumbersome due to the presence of zero terms in the diagonal of the global stiffness matrix (see eq. (9)). This requires the use of adequate solvers or regularization techniques. For this reason the use of an alternative "simpler" penalty approach has been successfully explosed. This approach is presented in next section.

2.4 Penalty Formulation

The basis of the penalty approach is to write the incompressibility condition as

$$\dot{\varepsilon}_{ii} = \frac{p}{\lambda} \tag{11}$$

where λ is a large number.

Obviously as λ increases the value of $\dot{\varepsilon}_{ii}$ tends to zero and in the limit $(\lambda \to \infty)$ the incompressibility condition is satisfied

$$u\frac{d\phi}{dx} - k\frac{d^2\phi}{dx^2} = Q(x) \quad , \quad 0 < x < L$$

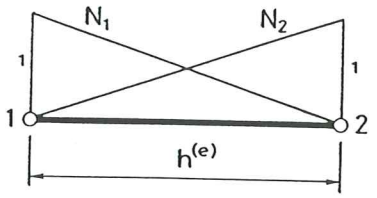

$$W_i = N_i + \frac{\alpha^{(e)} h^{(e)}}{2} \frac{\partial N_i}{\partial x}$$

$$\alpha^{(e)} = \coth(\gamma) - \frac{1}{\gamma} \quad , \quad \gamma = \frac{u h^{(e)}}{2k}$$

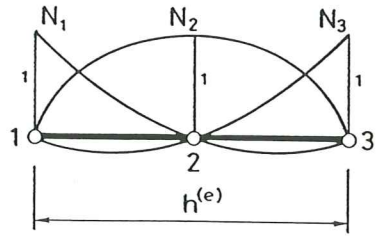

$$W_i = N_i + \frac{\alpha h^{(e)}}{2} \frac{\partial N_i}{\partial x} \quad , \quad i = 1,3$$

$$W_i = N_i + \frac{\beta h^{(e)}}{2} \frac{\partial N_i}{\partial x} \quad , \quad i = 2$$

$$\alpha = \frac{(3+3\gamma\beta)\tanh\gamma - (3\gamma+\gamma^2\beta)}{(2-3\beta\tanh\gamma)\gamma^2}$$

$$\beta = \frac{1}{2}(\coth\frac{\gamma}{2} - \frac{2}{\gamma})$$

Figure 2 Upwinding weighting functions for linear and quadratic 1D elements [5], [10]

Eq.(11) allows to eliminate the pressure as

$$p = \lambda \dot{\varepsilon}_{ii} = \lambda \mathbf{m}^T \dot{\boldsymbol{\varepsilon}} = \lambda \mathbf{m}^T \mathbf{L}\mathbf{u} = \lambda \mathbf{m}^T \mathbf{B}\bar{\mathbf{u}} \tag{12}$$

Substituting (12) in (1a) the momentum equation can be rewritten in terms of velocities only as

$$W_i = N_i + \frac{\alpha^{(e)} h^{(e)}}{2\|\mathbf{u}\|} \mathbf{u}^T \nabla N_i$$

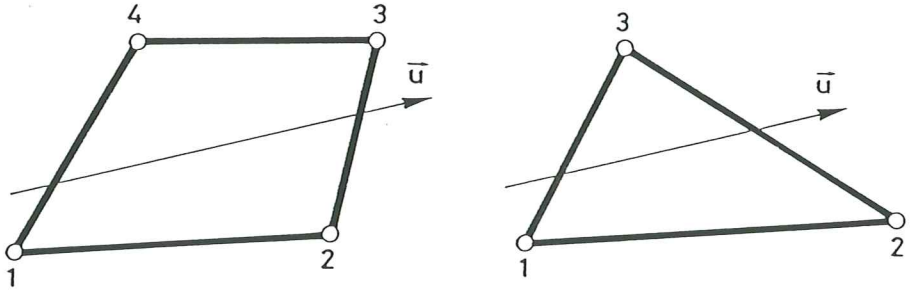

$\alpha^{(e)}$ as for 1D elements with $k = \frac{u_i k_{ij} u_j}{\|\mathbf{u}\|^2}$ and $h^{(e)} = \frac{\|\mathbf{u}\|}{\|\mathbf{u}_N\|} h_N$

$\mathbf{u}_N$= velocity in the parent domain

h_N=2 quadrilaterals, =1 for triangles

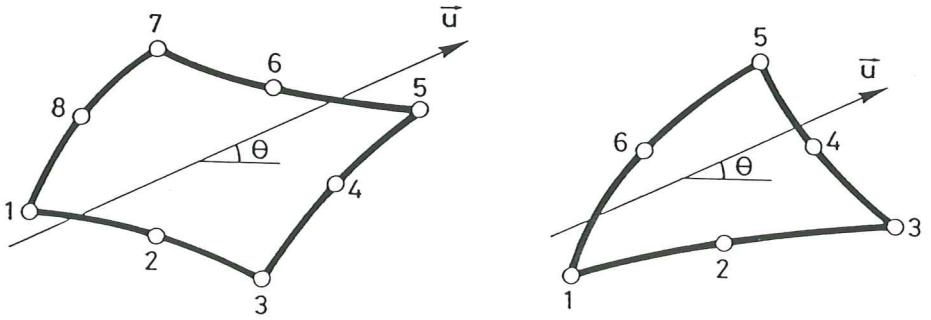

$$\alpha_i^{(e)} = f_i(\theta)\alpha + [1 - f_i(\theta)]\beta$$

Quadrilaterals

$f_i(\theta) = 1,\ i = 1,3,5,7$

$f_2(\theta) = f_6(\theta) = \sin^2\theta$

$f_4(\theta) = f_8(\theta) = \cos^2\theta$

Triangle

$f_i(\theta) = 1,\ i = 1,3,5$

$f_2(\theta) = \sin^2\theta,\ f_6(\theta) = \cos^2\theta$

$f_4(\theta) = f_2(\theta - \frac{\pi}{4})$

α, β as in Figure 1 ; k and $h^{(e)}$ as above

Figure 3 Upwinding weighting functions for linear and quadratic triangular and quadrilateral elements [5].

$$\boxed{\rho\left[\frac{\partial \mathbf{u}}{\partial t}+(\nabla \mathbf{u}^T)^T\mathbf{u}\right]+\mathbf{L}^T\mathbf{m}(\lambda\mathbf{m}^T\mathbf{L}\mathbf{u})-\mathbf{L}^T\mathbf{D}\mathbf{L}\mathbf{u}-\mathbf{b}_0=\mathbf{0}} \tag{13}$$

After adequate (SUPG) weighting and discretization of the velocity field the following equation system is obtained

$$\mathbf{M}\dot{\bar{\mathbf{u}}}+[\mathbf{K}+\bar{\mathbf{K}}+\lambda\hat{\mathbf{K}}]\bar{\mathbf{u}}=\mathbf{f} \tag{14}$$

where the new matrix

$$\hat{\mathbf{K}}_{ij}^{(e)}=-\int_\Omega\left\{[\mathbf{m}^T\bar{\mathbf{B}}_i]^T\mathbf{m}^T\mathbf{B}_j-[\bar{\mathbf{W}}_{u_i}]^T\mathbf{L}^T\mathbf{m}\mathbf{m}^T\mathbf{B}_j\right\}d\Omega \tag{15}$$

Note that only for the Galerkin weighting ($\mathbf{W}_u=\mathbf{N}_u$ and $\bar{\mathbf{W}}_u=\mathbf{0}$) matrix $\hat{\mathbf{K}}$ and the system (14) are symmetric.

For steady state eq.(14) reads

$$[\mathbf{K}+\bar{\mathbf{K}}+\lambda\hat{\mathbf{K}}]\bar{\mathbf{u}}=\mathbf{f} \tag{16a}$$

which for $\lambda\rightarrow\infty$ gives

$$\hat{\mathbf{K}}\bar{\mathbf{u}}=\frac{1}{\lambda}\mathbf{f}=\mathbf{0} \tag{16b}$$

Obviously, the non trivial solution ($\bar{\mathbf{u}}\neq 0$) requires matrix $\hat{\mathbf{K}}$ to be singular [37]. Singularity of $\hat{\mathbf{K}}$ can be achieved via *reduced integration* techniques or via *assumed presure distributions* techniques. The use of reduced integration procedures has been very popular in last decade amongst finite element practitioners. A full description of this technique can be found in [37]. However, it is widely acknowleged today that this approach has a certain number of disadvantages, like the possibility of introducing internal mechanisms in the element which can polute the solution.

The alternative is to prescribe "a priori"a pressure field, satisfying eq.(9), as

$$p=\mathbf{N}_p\bar{\mathbf{p}} \tag{17}$$

where $\bar{\mathbf{p}}=[p_1,p_2,\cdots,p_{n_p}]^T$ contains the values of the pressure at n_p specified points and $\mathbf{N}_p$ are interpolating basis functions.

Now using the penalty condition (11) we can express (17) in terms of the nodal velocity parameters as

$$p=\lambda\mathbf{N}_p\mathbf{m}^T\mathbf{B}^p\bar{\mathbf{u}}=\lambda\hat{\mathbf{B}}\bar{\mathbf{u}} \tag{18a}$$

with

$$\hat{\mathbf{B}} = \mathbf{N}_p \mathbf{m}^T \mathbf{B}^p \tag{18b}$$

In (18b) $\mathbf{B}^p$ is the strain-rate matrix computed at the n_p points where the pressure variables $\bar{\mathbf{p}}$ have been specified.

The final form of the penalty matrix $\hat{\mathbf{K}}$ in (15) reads now

$$\hat{\mathbf{K}}_{ij}^{(e)} = \int_\Omega [\mathbf{m}^T \bar{\mathbf{B}}_i]^T \hat{\mathbf{B}}_j d\Omega \tag{19}$$

Note that $\hat{\mathbf{K}}$ is now always non symmetric. However, this approach yields good results providing a compatible pressure field is chosen [37].

An alternative procedure based on the same concepts is to introduce the penalty parameter in the $\mathbf{u}-p$ formulation so that the incompressibility equation reads now

$$\int_\Omega W_p \left[\frac{1}{\lambda} p + \mathbf{m}^T \mathbf{L} \mathbf{u} \right] d\Omega = 0 \tag{20}$$

Choosing now a compatible interpolation for pressures and velocities, the system of eqs.(8) can be written for the stationary case as

$$\begin{bmatrix} \mathbf{K} + \bar{\mathbf{K}} & \mathbf{K}^p \\ \bar{\mathbf{K}}^p & \frac{1}{\lambda}\mathbf{C} \end{bmatrix} \begin{Bmatrix} \bar{\mathbf{u}} \\ \bar{\mathbf{p}} \end{Bmatrix} = \begin{Bmatrix} \mathbf{f} \\ \mathbf{0} \end{Bmatrix} \tag{21}$$

where $\mathbf{C} = \int_\Omega \mathbf{N}_p^T \mathbf{N}_p d\Omega$.

The second row of equations allows to eliminate the pressures as $\bar{\mathbf{p}} = -\lambda \mathbf{C}^{-1} \bar{\mathbf{K}}^p \bar{\mathbf{u}}$. Substitution of this value in the first row yields a final system of equations identical to (16a) with $\hat{\mathbf{K}}$ given by

$$\hat{\mathbf{K}} = -\mathbf{K}^p \mathbf{C}^{-1} \bar{\mathbf{K}}^p \tag{22}$$

thus allowing a solution involving the nodal velocities $\bar{\mathbf{u}}$ only.

It can be proved that matrix $\hat{\mathbf{K}}$ of (22) is singular if the condition (9) is satisfied, thus ensuring the existance of the solution for $\lambda \to \infty$.

2.5 Pressure recovery in the penalty formulation

In the penalty method the velocities are the only independent variables and the pressure has to be computed "a posteriori" from the known velocity field. The simpler option is to compute the pressure via the incompressibility condition (eq.(12)).

This method is inaccurate as it implies multiplication of a very large number (λ) and the value of the volumetric strain rate which should be as close as zero is possible.

An alternative procedure exploited by Sohn and Heinrich [29] is to compute the pressure by solving a Laplacian form derived from the momentum and continuity equations. Thus, by differentiating the x and y momentum equations with respect to x and y, respectively and substituting the result in the continuity equation, one gets

$$\left(\frac{\partial^2}{\partial x^2}+\frac{\partial^2}{\partial y^2}\right)p=-\frac{\partial}{\partial x}(\mathbf{u}^T\nabla\mathbf{u})-\frac{\partial}{\partial y}(\mathbf{u}^T\nabla\mathbf{u}) \tag{23}$$

Solution of (23) using standard FEM yields correct values for the pressure distributions. Note, however, that (23) involves second derivatives of the velocity field. This presents no difficulty when second or higher order approximations for $\mathbf{u}$ are used. However, for linear elements the second derivatives of $\mathbf{u}$ must be computed via a smoothing technique of the discontinuous first derivative field [29].

2.6 Transient solutions using the penalty approach

It is known that explicit algorihms are unconditionally unstable when the solution of the initial value problem (7a) is attempted. In order to avoid the need for solving large implicit systems, several authors have proposed the use of algorithms that uncouple the velocity and pressure fields and then correct iteratively velocities and pressures. The differential equation for the velocity may be solved explicitly, whereas implicit algorithms have to be used for the pessure equation (see, e.g. [2'], [8']).

In other cases, pressures are eliminated "a priori"through the penalty equation, thus leading to an equation involving velocities only. When the penalty parameter tends to infinity explicit algorithms become unconditionally unstables, and the use of implicit schemes is mandatory. A popular integration method is the generalized trapezoidal rule. For a general nonlinear systems of the form

$$\dot{x}=F(x,t) \tag{24}$$

F being a nonlinear vector functions and $x=x(t)$ the vector of nodal unknowns, this method reads: given x^n, find x^{n+1} satisfying

$$x^{n+1}-x^n=\Delta t\theta F^{n+1}(x,t)+\Delta t(1-\theta)F^n(x,t) \tag{25a}$$

where Δt is the time step increment, θ a parameter ($0\leq\theta\leq 1$), x^k the unknown at $t^k=\kappa\Delta t$ and

$$F^k(x,t)\equiv F(x^k,t^k) \tag{25b}$$

For $\theta = 0$, the scheme is known as the explicit Euler method (unconditionally unstable for the incompressible Navier–Stokes equations), for $\theta = 1/2$ as the Crank–Nicolson method (unconditionally stable and second order accurate) and for $\theta = 1$ as the backward or full implicit Euler method (first order accurate and unconditionally stable).

In our numerical experiments, we have observed that the increased accuracy obtained with $\theta = 1/2$ compensates the cost of evaluating the term $F^n(x,t)$ in (25a) when results are compared with the choice $\theta = 1$. However, if x^1 is computed from x^0 (the initial condition) using $\theta = 1/2$, oscillations are found that may pollute the solution for several time steps. This is due to the inability of the (finite) time increments to resolve the rapidly oscillating harmonics associated with the time expansion of the unknown $x(t)$. This problem is solved using $\theta = 1$ in the first time step (thus damping those harmonics) and $\theta = 1/2$ for the following.

With this considerations in mind, an scheme for solving the ordinary differential equation (14) could read as follows:

1. Assume $\bar{\mathbf{u}}^0$ be given (initial condition).
2. Find $\bar{\mathbf{u}}^1$ solving.

$$\begin{aligned}&[\mathbf{M} + \Delta t(\mathbf{K} + \bar{\mathbf{K}}(\bar{\mathbf{u}}^1) + \lambda\hat{\mathbf{K}})]\bar{\mathbf{u}}^1 = \\ &= \Delta t\mathbf{f}^1 + \mathbf{M}\bar{\mathbf{u}}^0\end{aligned} \tag{26a}$$

3. Fix $\theta(\theta = 1/2$, for example). For $n = 1, 2, \cdots, N$ (total number of time steps), find $\bar{\mathbf{u}}^{n+1}$ solving.

$$\begin{aligned}&[\mathbf{M} + \Delta t\theta(\mathbf{K} + \bar{\mathbf{K}}(\bar{\mathbf{u}}^{n+1}) + \lambda\hat{\mathbf{K}})]\bar{\mathbf{u}}^{n+1} \\ &= \Delta t\mathbf{f}^{n+1} + (1-\theta)\Delta t\mathbf{f}^n + \\ &+ [\mathbf{M} - (1-\theta)\Delta t(\mathbf{K} + \bar{\mathbf{K}}(\bar{\mathbf{u}}^n) + \lambda\hat{\mathbf{K}})]\bar{\mathbf{u}}^n\end{aligned} \tag{26b}$$

The nonlinear systems (26a) and (26b) can be solved using either Picard or Newton–Raphson iterations. Usually, only in the first time steps several iterations are required. In that case, one or two initial Picard iterations can be performed in order to obtain a good initial iterate for the Newton–Raphson scheme.

In Section 6 we present some examples of application of the penalty formulation presented.

2.7 Alternatives for circumventing the restrictions of u/p formulation

In Section 2.2 we have seen that the requirements of solvability pose dificulties in the use of arbitrary finite element interpolations. These conditions emerge due to the zero diagonal term in eq.(8) which yields a singular system

unless, for any assemble of elements, the number of variables of $\bar{\mathbf{u}}$ is larger than that of $\bar{\mathbf{p}}$.

Avoidance of this difficulty by use of penalty forms (and reduced integration) which introduce a small non-zero term in the diagonal as shown in previous sections, is not robust and it is doomed to failure, unless *a priori* the L.B.B. conditions are satisfied. For this reason alternative stabilization methods are needed [2]. Hughes *et al.* [14] have shown for Stokes flow that such stabilization can be achieved by the following weighting of the continuity equation

$$\int_\Omega N_p \nabla^T \mathbf{u} d\Omega + \int_\Omega \frac{\alpha^{(e)}(h^{(e)})^2}{2\mu} [\nabla N_p]^T [\underline{-\mathbf{L}^T \mathbf{D} \mathbf{L} \mathbf{u}} + \underline{+ \mathbf{L}^T \mathbf{m} \mathbf{p}} - \mathbf{b}_0] \, d\Omega = 0 \tag{27}$$

where $\alpha^{(e)}$ is a parameter similar to that of eq.(10a) for the SUPG formulation and $h^{(e)}$ is again a mesure of the element size [14].

Eq.(27) differs from the standard Galerkin approximation by the addition of the second integral in (27). This integral can be added as the underlined terms in (27) are nothing else than the momentum equation which is already approximated via eq.(3) (neglecting inertia terms).

After standard $\mathbf{u} - p$ discretization eqs.(3) and (27) lead to the following system

$$\begin{bmatrix} \mathbf{K} & \mathbf{K}^p \\ (\bar{\mathbf{K}}^p - \mathbf{L}) & \mathbf{H} \end{bmatrix} \begin{Bmatrix} \bar{\mathbf{u}} \\ \bar{\mathbf{p}} \end{Bmatrix} = \begin{Bmatrix} \bar{\mathbf{f}} \\ \mathbf{g} \end{Bmatrix} \tag{28}$$

where the new matrices $\mathbf{L}$, $\mathbf{H}$ and $\mathbf{g}$ are given by

$$\begin{aligned} \mathbf{H} &= \int_\Omega \frac{\alpha^{(e)}(h^{(e)})^2}{2\mu} [\nabla N_p]^T \mathbf{L}^T \mathbf{m} \mathbf{N}_p d\Omega \\ \mathbf{L} &= \int_\Omega \frac{\alpha^{(e)}(h^{(e)})^2}{2\mu} [\nabla N_p]^T \mathbf{L}^T \mathbf{D} \mathbf{B} d\Omega \\ \mathbf{g} &= \int_\Omega \frac{\alpha^{(e)}(h^{(e)})^2}{2\mu} [\nabla N_p]^T \mathbf{b}_0 d\Omega + \text{boundary terms} \end{aligned} \tag{29}$$

Note that eq.(28) can now be directly solved with any equation solution scheme and the need for different appoximations for $\mathbf{u}$ and p dissappears.

Sampaio [27] has presented a formulation similar to the above by combination of the application of Galerkin method to the steady state continuity equation with the least square method to the discretized momentum equation. In doing so the parameter $\alpha^{(e)}$ in (27) comes naturally from the time

discretization and thus can be chosen to correspond to the stability limit of time step, which has proved to give optimal upwinding for convection-diffusion problems.

More recently Zienkiewicz and Wu [36] have shown how an equation system of the form (28) can be obtained by seeking the stady state solution through the use of various time marching schemes like Taylor-Galerkin, Runge-Kutta, etc. Unfortunally in all cases the steady state equations arrived are unsymmetric (see eq.(28)). This brings additional cost if the steady state equation is solved directly, but it is of no importance of time step iterative solvers are used. This has been observed already by Schneider *et al.* [28] and Kawahava *et al.* [16], when using the so called "velocity correction method" for solution of steady state incompressible flows.

3. A FINITE VOLUME $\mathbf{u}-p$ AND PENALTY FORMULATIONS

The finite volume method evolved in the early seventies via finite difference approximations and today has many proponents amongst CFD practitioners [17,18,26]. Comprenhensive descriptions of the finite volume techniques are given by Patankar [21] and Hirsch [11]. Recently Zienkiewicz and Oñate [38] have shown that finite volume equations can be derived as a particular case of standard finite element approximations. This fact can be easly exploited to derive alternative finite volume formulations from the ones described in previous sections. Research in this field is currently under development at the authors's institution.

The basis of the finite volume method is the choice of unit weighting functions within the analysis domain. Thus setting $\mathbf{W}_u = \mathbf{I}$ in eq.(3) and applying the divergence theorem to the term $(\nabla \mathbf{u}^T)^T \mathbf{u}$ yields

$$\int_\Omega \rho \frac{\partial \mathbf{u}}{\partial t} d\Omega + \oint_\Gamma \mathbf{M} \begin{Bmatrix} u^2 \\ v^2 \\ uv \end{Bmatrix} d\Gamma - \oint_\Gamma \mathbf{t} d\Gamma - \int_\Omega \mathbf{b} d\Omega = \mathbf{0} \tag{30}$$

where the boundary tractions $\mathbf{t}$ are obtained as

$$\mathbf{t} = \mathbf{M}\boldsymbol{\sigma} = \mathbf{M}(\mathbf{D}\mathbf{L}\mathbf{u} - \mathbf{m}p) \tag{31}$$

The continuity equation (4) takes the following form, after application of the divergence theorem

$$\oint_\Gamma \mathbf{n}^T \mathbf{u} d\Gamma = 0 \tag{32}$$

In (30) and (32) $\mathbf{n} = [n_x, n_y]^T$ is the normal vector to the external boundary Γ and $\mathbf{M} = \begin{bmatrix} n_x & 0 & n_y \\ 0 & n_y & n_x \end{bmatrix}$.

The domain can now be discretized in finite elements in the standard form with interpolation of velocities and pressure given by eq.(6).

The discretized form of equations (30) and (32) can now be applied to the control domain (finite volume) surrounding each node in the finite element mesh. This gives for each control domain "v" the following system of equations

$$\mathbf{M}^{(v)}\dot{\mathbf{a}}^{(v)} + \bar{\mathbf{f}}^{(v)} + \mathbf{f}^{(v)} = \mathbf{0} \tag{33}$$

where

$$\mathbf{M}^{(v)} = \begin{bmatrix} \hat{\mathbf{M}}^{(v)} & \mathbf{0} \\ \mathbf{0} & \mathbf{0} \end{bmatrix} \quad ; \quad \hat{\mathbf{M}}^{(v)} = \int_{\Omega^{(v)}} \mathbf{N}_u d\Omega \tag{34a}$$

$$\bar{\mathbf{f}}(v) = \begin{Bmatrix} \mathbf{f}_m^{(v)} \\ \mathbf{f}_c^{(v)} \end{Bmatrix} \quad ; \quad \mathbf{a}^{(v)} = \begin{Bmatrix} \bar{\mathbf{u}} \\ \bar{\mathbf{p}} \end{Bmatrix}^{(v)} \tag{34b}$$

with

$$\mathbf{f}_m^{(v)} = \frac{1}{2}\oint_{\Gamma^{(v)}} \mathbf{M}\mathbf{N}_u(\bar{\mathbf{u}})^2 d\Gamma - \oint_{\Gamma^{(v)}} \mathbf{M}[\mathbf{D}\mathbf{B}\bar{\mathbf{u}} - \mathbf{m}\mathbf{N}_p\bar{\mathbf{p}}]\, d\Gamma \tag{34c}$$

$$\mathbf{f}_c^{(v)} = \oint_{\Gamma^{(v)}} \mathbf{n}^T[\mathbf{N}_u\bar{\mathbf{u}}]d\Gamma \tag{34d}$$

and $$\mathbf{f}^{(v)} = -\oint_{\Omega^{(v)}} \mathbf{b}d\Omega \tag{34e}$$

In (34) $\Omega^{(v)}$ and $\Gamma^{(v)}$ are the area and boundary of the control domain chosen and $(\bar{\mathbf{u}})_i^2 = \left[(u_i)^2, (v_i)^2, u_i v_i\right]^T$. Note that the computation of the "flux" vectors $\hat{\mathbf{f}}_m^{(v)}$ and $\hat{\mathbf{f}}_c^{(v)}$ now involve only integrals along the domain boundary.

Figure (4) shows some examples of control domains based on linear triangles leading to standard "vertex centered" and "cell centered" finite volume schemes [11], [21]. Examples of control domains using higher order interpolations in quadrilateral or triangular meshes are shown in Figure 5.

Equations (33) can now be solved in time using any explicit/implicit integration scheme.

If the *penalty approach* is used the finite volume equations are simplified simply by making

$$\mathbf{M}^{(v)} = \hat{\mathbf{M}}^{(v)} \quad ; \quad \hat{\mathbf{f}}^{(v)} = \hat{\mathbf{f}}_m^{(v)} \tag{35}$$

and substituting the pressure term in (34c) by $\alpha\mathbf{m}^T\mathbf{B}\bar{\mathbf{u}}$ where the strain rate matrix $\mathbf{B}$ can be obtained by any of the different alternatives explained in Section 2.4.

Further research in this area is currently under development and it will be reported in a near future.

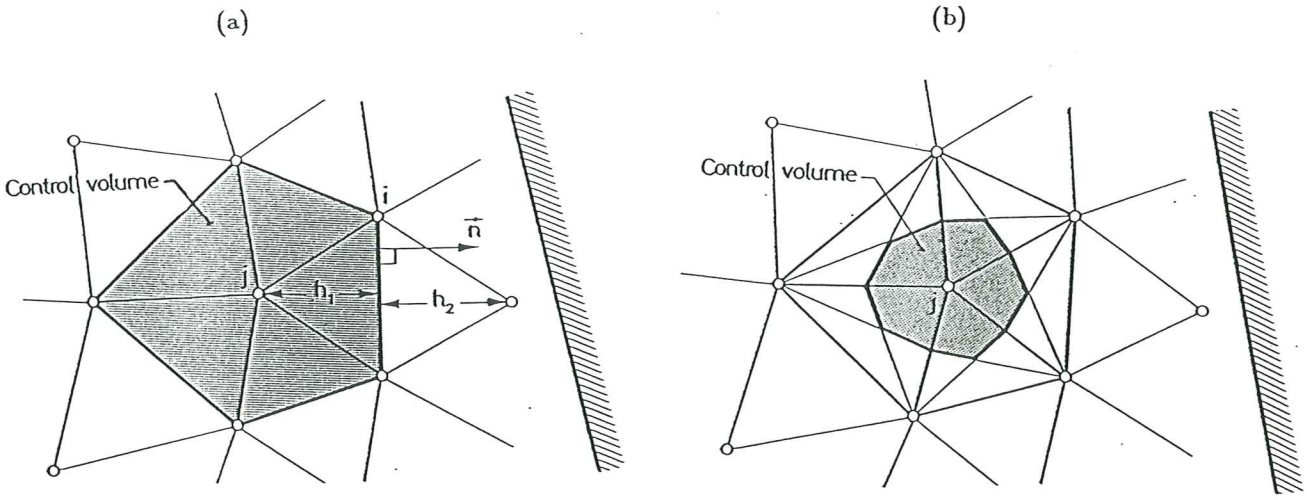

Figure 4 Control volumes for "vertex centered" (a) and "cell centered" (b) finite volume schemes.

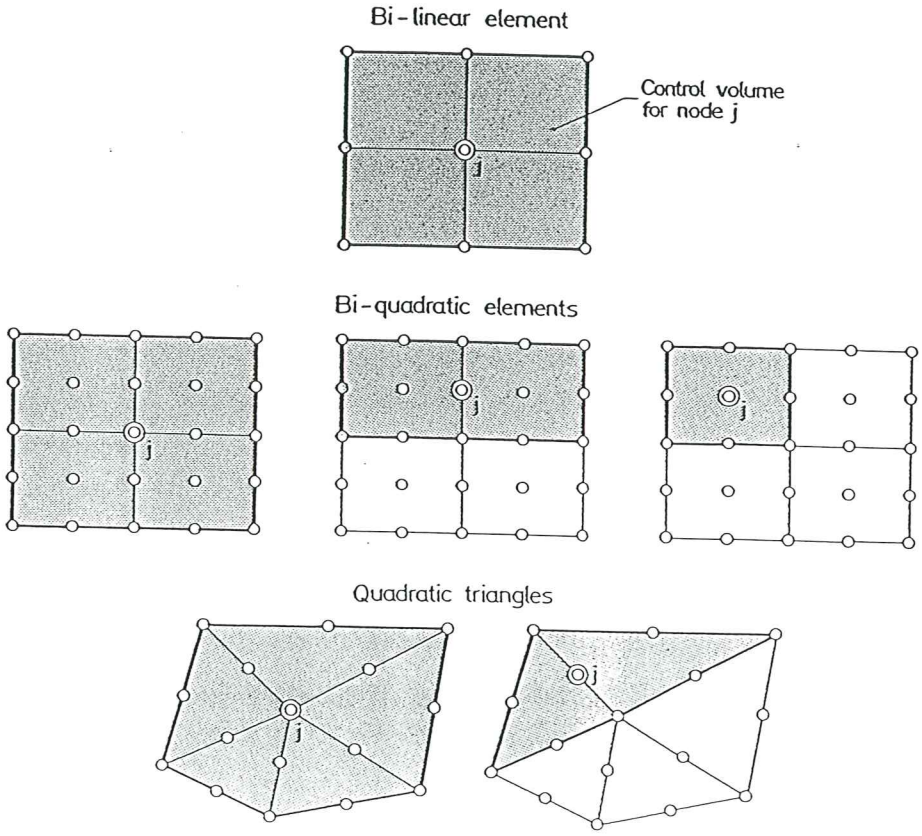

Figure 5 Examples of control domains using higher order interpolations in triangular or quadrilateral meshes.

4. COMPRESSIBLE FLOW

4.1 Basic equations

For compressible flow conditions the Navier-Stokes can be written in the following conservation form

$$\frac{\partial \mathbf{u}}{\partial t} + \frac{\partial \mathbf{f}_i}{\partial \mathbf{x}_i} + \frac{\partial \mathbf{g}_i}{\partial \mathbf{x}_i} + \mathbf{q} = 0 \tag{36}$$

for 2D problems

$$\begin{aligned}
\mathbf{u} &= [\rho, \rho u_1, \rho u_2, \rho E]^T \\
\mathbf{f}_i &= [\rho u_i, \rho u_i u_1 + p\delta_{1i}, \rho u_i u_2 + p\delta_{2i}, (\rho E + p)u_i]^T \\
\mathbf{g}_i &= [0, -\tau_{1i}, -\tau_{2i}, -\tau_{3i}, \frac{\partial}{\partial x_i}(-\tau_{ij}u_j) - k\frac{\partial T}{\partial x_i}]^T \\
\mathbf{q} &= -[0, b_1, b_2, b_3, 0]^T
\end{aligned} \tag{37}$$

with

$$\begin{aligned}
\tau_{ij} &= \mu\left[\frac{\partial u_i}{\partial x_j} + \frac{\partial u_j}{\partial x_i} - \frac{2}{3}\frac{\partial u_k}{\partial x_k}\right] \\
p &= RT\rho
\end{aligned} \tag{38}$$

In above all terms have been previously defined except, k, R, T and E which are the thermal conductivity, the universal gas constant, the temperature and the total energy, respectively.

The inviscid form of the compressible flow equations (Euler equations) is simply obtained neglecting the contribution of vector $\mathbf{g}$ in (36). Also for adiabatic conditions the energy terms are neglected in (36)–(37).

4.2 Transition from incompressible to compressible flow

Eq.(36) can be written omitting energy terms as

Continuity:
$$\frac{\partial \rho}{\partial t} + \frac{\partial(\rho u_i)}{\partial x_i} = 0 \tag{39}$$

Momentum:
$$\frac{\partial(\rho u_i)}{\partial t} + \frac{\partial(\rho u_i u_j)}{\partial x_j} + \frac{\partial p}{\partial x_i} - \frac{\partial \tau_{ij}}{\partial x_j} - b_i = 0 \tag{40}$$

Substracting (40)–(39) and rearranging terms we can write

$$\frac{\partial \rho}{\partial t} + \rho \frac{\partial u_i}{\partial x_i} + \boxed{\frac{\partial \rho}{\partial x_i} u_i} = 0 \tag{41}$$

$$\rho \left(\frac{\partial u_i}{\partial t} + u_j \frac{\partial u_i}{\partial x_j} \right) - \tau_{ij} + \frac{\partial p}{\partial x_i} - b_i = 0 \tag{42}$$

The steady form of above equations is identical to that of *incompressible flow* (see Section 2.1) if the bracked term $\frac{\partial \rho}{\partial x_i} u_i = 0$. Clearly this will happen in zones where small velocities ($u_i \rightarrow 0$) or small density changes occur ($\frac{\partial \rho}{\partial x_i} \rightarrow 0$).

Therefore, numerical finite elements (or finite volumes) algorithms to model compressible flow problems should be robust enough to predict accurately the behaviour in global or local incompressible flow zones. Thus, all considerations for element and algorithm design, made in previous sections for incompressible flow are again applicable.

4.3 Petrov-Galerkin finite element models for compressible flows

The spatial weighted residual form of eq.(36) can be written in standard form as

$$\int_\Omega \mathbf{W}^T \left[\frac{\partial \mathbf{u}}{\partial t} + \frac{\partial \mathbf{f}_i}{\partial \mathbf{x}_i} + \frac{\partial \mathbf{g}_i}{\partial \mathbf{x}_i} + \mathbf{q} \right] d\Omega = 0 \tag{43}$$

The unknown vector $\mathbf{u}$ can now be interpolated using finite element shape functions $\mathbf{N}$ as

$$\mathbf{u} = \mathbf{N}\mathbf{a} \tag{44}$$

Eq.(44) allows to obtain the relationship between the flux vectors $\mathbf{f}$ and $\mathbf{g}$ and the nodal unknow parameters $\mathbf{a}$ through (37) and (38) as

$$\mathbf{f}_i = \mathbf{f}_i(\mathbf{a}) \quad ; \quad \mathbf{g}_i = \mathbf{g}_i(\mathbf{a}) \tag{45}$$

Substitution of (44) and (45) in (43) and integrating by parts the flux terms allows to obtain the discretized system of equations in the form

$$\mathbf{M}\dot{\mathbf{a}} + \mathbf{f}_a + \mathbf{p} = \mathbf{0} \tag{46}$$

where

$$\mathbf{M} = \int_\Omega \mathbf{W}^T \mathbf{N} d\Omega \tag{47a}$$

$$\mathbf{f}_a = -\int_\Omega \frac{\partial \mathbf{W}^T}{\partial \mathbf{x}_i}(\mathbf{f}_i + \mathbf{g}_i)d\Omega \tag{47b}$$

$$\mathbf{p} = \int_\Omega \mathbf{W}^T \mathbf{b} d\Omega + \oint_\Gamma \mathbf{W}^T(\mathbf{f}_i + \mathbf{g}_i)n_i d\Gamma \tag{47c}$$

where $n_1 = n_x$ and $n_2 = n_y$ are the components of the unit normal vector.

Different choices for the weighting functions $\mathbf{W}$ are of course now possible. The obvious Galerkin choice ($\mathbf{W} = \mathbf{N}$) should however be disregarded as it leads to numerical instabilities of the type mentioned in Section 2.2.

The usual practice is to choose a SUPG weighting similar to that of eq.(11a) with

$$\mathbf{W} = \mathbf{N} + \frac{1}{2\|\mathbf{u}\|}[\alpha h]\mathbf{u}^T \nabla \mathbf{N} \tag{48a}$$

where

$$[\alpha h] = \begin{bmatrix} \alpha_\rho h_\rho & & & \mathbf{0} \\ & \alpha_u h_u & & \\ & & \alpha_v h_v & \\ \mathbf{0} & & & \alpha_\varepsilon h_\varepsilon \end{bmatrix} \tag{48b}$$

The form of the upwinding parameters for each of the equations is shown in Table III [3']. In most cases the option $h_\rho = h_u = h_v = h_\varepsilon = h^{(e)}$ where $h^{(e)}$ is a characteristic element lenght is taken. It is interesting to note that for the steady-state case and $\mathbf{q} = 0$ the Petrov-Galerkin weighting with a linear finite element interpolations is again equivalent to adding a diffussion along the velocity stream lines [3].

Brueckner [3] and Brueckner and Heinrich [3'] have shown that eq.(48a) holds only if the energy and constitutive equations are written in terms of the specific energy. However if the expression of the total energy is used, the convective velocity is different for each flow equation. This implies that both eq.(48a) and the upwinding parameters must be subsequently modified.

The SUPG approach, together with adequate finite element interpolation and time integration schemes, seems to be an efficient procedure for solving high speed compressible flow problems. Some examples of application of this technique can be found in [3,3'].

The above procedure can be refined by means of adding shock capturing terms [12–15] and using adaptive refinement techniques as explained is Section 5. However, it has been shown that Petrov-Galerkin models have an inherent capacity to capture shocks and no further addition of extra viscous terms seems to be needed [3,3']. This point will certainly be subject of debate and further research in the near future.

$$\alpha_\rho = 1$$

$$\alpha_\rho = \coth\frac{\gamma u}{2} + \frac{2}{\gamma_u} \quad , \qquad \gamma_u = \frac{\rho Re}{1 + \frac{u^2}{3\|\mathbf{u}\|^2}}\|\mathbf{u}\|h_u$$

$$\alpha_v = \coth\frac{\gamma v}{2} + \frac{2}{\gamma_v} \quad , \qquad \gamma_v = \frac{\rho Re}{1 + \frac{v^2}{3\|\mathbf{u}\|^2}}\|\mathbf{u}\|h_v$$

$$\alpha_\varepsilon = \coth\frac{\gamma_\varepsilon}{2} + \frac{2}{\gamma_\varepsilon} \quad , \qquad \gamma_\varepsilon = \frac{\rho Pr Re}{\gamma}\|\mathbf{u}\|h_\varepsilon$$

Re = Reynolds number , Pr = Prandtl number

γ= ratio of specific heats. Usually $h_u = h_v = h_\varepsilon = h^{(e)}$

Table III. Typical upwinding parameters for compressible flow [3,3'].

4.4 Taylor-Galerkin approach for Euler equations

To explain the basis of the Taylor-Galerkin approach we will consider first the inviscid (Euler) form of eq.(36) with no source terms, i.e.

$$\frac{\partial \mathbf{u}}{\partial t} + \frac{\partial \mathbf{f}_i}{\partial \mathbf{x}_i} = 0 \tag{49}$$

A Taylor expansion in time of the unknown $\mathbf{u}$ is performed first as

$$\mathbf{u}^{n+1} = \mathbf{u}^n + \Delta t \left(\frac{\partial u}{\partial t}\right)^n + \frac{\Delta t^2}{2}\left(\frac{\partial^2 \mathbf{u}}{\partial t^2}\right)^n \tag{50}$$

From (49) we can obtain

$$\frac{\partial \mathbf{u}}{\partial t} = -\frac{\partial \mathbf{f}_i}{\partial \mathbf{x}_i} \quad ; \quad \frac{\partial^2 \mathbf{u}}{\partial t^2} = \frac{\partial}{\partial x_i}\left(\mathbf{A}_i \frac{\partial \mathbf{f}_k}{\partial \mathbf{x}_k}\right) \tag{51a}$$

with

$$\mathbf{A}_i = \frac{\partial \mathbf{f}_i}{\partial \mathbf{u}} \tag{51b}$$

Substituting (50b) in (50a) we can rewritte (50a) as

$$\Delta \mathbf{u}^n = -\Delta t \left(\frac{\partial \mathbf{f}_i}{\partial \mathbf{x}_i}\right)^n + \frac{\Delta t^2}{2}\frac{\partial}{\partial \mathbf{x}_i}\left(\mathbf{A}_i \frac{\partial \mathbf{f}_k}{\partial \mathbf{x}_k}\right)^n \tag{52}$$

Note that the Δt^2 terms in (52) can be interpreted as a balancing diffusion added to the original equations (49).

A finite interpolation can now be chosen where the incremental unknowns $\Delta \mathbf{u}^n$ are interpolated from the nodal values $\Delta \mathbf{a}_i^n$ by

$$\Delta \mathbf{u} = \sum \mathbf{N}_i \Delta \mathbf{a}_i^n \tag{53}$$

with $\mathbf{N}_i = N_i \mathbf{I}$ where N_i is the shape function of ith node.

The Galerkin weighted residual form of eq.(52) is written next as

$$\int_\Omega \mathbf{N}_j^T \Delta \mathbf{u}^n d\Omega = -\int_\Omega \mathbf{N}_j^T \Delta t \left(\frac{\partial \mathbf{f}_i}{\partial \mathbf{x}_i} \right)^n d\Omega + \frac{\Delta t^2}{2} \int_\Omega \mathbf{N}_j^T \frac{\partial}{\partial \mathbf{x}_i} \left(\mathbf{A}_i \frac{\partial \mathbf{f}_k}{\partial \mathbf{x}_k} \right) d\Omega \tag{54}$$

Integration by parts of the second integral in the right hand side of (53) leads to

$$\begin{aligned} \int_\Omega \mathbf{N}_j^T \Delta \mathbf{u}^n d\Omega = -\Delta t \int_\Omega \left[\mathbf{N}_j + \frac{\Delta t}{2} \mathbf{A}_i^n \frac{\partial N_j}{\partial \mathbf{x}_i} \right]^T \frac{\partial \mathbf{f}_k}{\partial \mathbf{x}_k} d\Omega + \\ + \oint_\Gamma \frac{\Delta t^2}{2} \mathbf{N}_j^T \mathbf{A}_i \frac{\partial \mathbf{f}_k}{\partial \mathbf{x}_k} n_k d\Gamma \end{aligned} \tag{55}$$

Substitution of the approximation (53) in (55) leads to a system of equations which can be written in the form

$$\mathbf{M} \Delta \mathbf{a}^n + \Delta t (\mathbf{f}_a + \mathbf{f})^n = 0 \tag{56}$$

with

$$\mathbf{M} = \int_\Omega \mathbf{N}^T \mathbf{N} d\Omega \quad ; \quad \mathbf{f}_a = \int_\Omega \left[\mathbf{N} + \frac{\Delta t}{2} \mathbf{A}_i \frac{\partial \mathbf{N}}{\partial \mathbf{x}_i} \right]^T \frac{\partial \mathbf{f}_k}{\partial \mathbf{x}_k} d\Omega \tag{57}$$

$$\text{and} \qquad \mathbf{f} = \oint_\Gamma \frac{\Delta t}{2} \mathbf{N}^T \mathbf{A}_i \frac{\partial \mathbf{f}_k}{\partial \mathbf{x}_k} n_k d\Gamma \tag{58}$$

The terms in brackets in the integral related to $\mathbf{f}_a$ can be interpreted as a weighting function

$$\mathbf{W} = \mathbf{N} + \frac{\Delta t}{2} \mathbf{A}_i \frac{\partial \mathbf{N}}{\partial \mathbf{x}_i} \tag{59}$$

Note the analogy of this expression with that of the upwind weighting function (11a). This provides an interesting analogy between the Petrov-Galerkin upwind parameters and the time increment entering in (59).

Eq.(56) can be solved in a single step for the values of $\Delta \mathbf{a}^n$ as

$$\Delta \mathbf{a}^n = -\Delta t \mathbf{M}^{-1}(\mathbf{f}_a + \mathbf{f})^n \tag{60}$$

from which the unknown values can be updated for the next time increment as $\mathbf{a}^{n+1} = \mathbf{a}^n + \Delta \mathbf{a}^n$. The full transient solution of (60) implies inverting the consistent mass matrix $\mathbf{M}$ for each time increment. However, if only the steady state solution is needed a "lumped" form of $\mathbf{M}$ can be used, thus allowing for a straight forward computation of $\Delta \mathbf{a}^n$ very adequate for coding in parallel processing systems.

Stability of the solution is controlled by the time increment shown in r.h.s of (60) which should be thus properly computed as to satisfy the standard stability requirements [37]. Peraire *et al.* [24,25] have successfully used a two-step solution of eq.(55) which avoids computation of matrix $\mathbf{A}_i$ at each increment.

Both one and two step algorithms are usually combined with a solution smoothing and the use of adaptive refinement techniques. Current research aims to the optimal definition of the time increment in (59) so that the minimum extra balancing diffussion is needed.

Zienkiewicz and Wu [36] have recently shown the intrinsic capability of the Taylor-Galerkin method for providing a system of equations of the form (28), thus overcoming the difficulties associated to the limit incompressible case as explained in Section 2.6. This allows the successfull use of this approach with elements with equal interpolation for all variables.

4.5 Taylor-Galerkin approach for viscous flows

Performing a Taylor expansions similar to that of eqs.(30) and using eq.(36) allows to obtain

$$\mathbf{u}^{n+1} = \mathbf{u}^n + \Delta t \left(\frac{\partial \mathbf{g}_j^n}{\partial \mathbf{x}_j} - \frac{\partial \mathbf{f}_j^n}{\partial \mathbf{x}_j} \right) + \frac{\Delta t^2}{2} \left[\frac{\partial}{\partial x_i} \left(\mathbf{A}_i \frac{\partial \mathbf{f}_k}{\partial \mathbf{x}_k} \right) - \mathbf{G} \frac{\partial \mathbf{f}_i}{\partial \mathbf{x}_i} \right]^n \tag{61}$$

where $\mathbf{A}_i = \frac{\partial \mathbf{f}_i}{\partial \mathbf{u}}$ and $\mathbf{G}_i = \frac{\partial \mathbf{g}_i}{\partial \mathbf{u}}$ are matrices of vector gradients and where derivatives or products of higher order than two have been neglected.

Eq.(61) can be now discretized using C_0 finite elements.

The Galerkin integral form of (61) can be written as

$$\begin{aligned} \int_\Omega \mathbf{N}^T \Delta \mathbf{u} d\Omega = \Delta t \int_\Omega \mathbf{N}^T \Bigg\{ & \frac{\partial \mathbf{g}_i^n}{\partial \mathbf{x}_i} - \\ & - \frac{\partial \mathbf{f}_i^n}{\partial \mathbf{x}_j} - \frac{\Delta t}{2} \left[\mathbf{G} \frac{\partial \mathbf{f}_i}{\partial \mathbf{x}_i} - \frac{\partial}{\partial \mathbf{x}_i} \left(\mathbf{A}_i \frac{\partial \mathbf{f}_k}{\partial \mathbf{x}_k} \right) \right]^n \Bigg\} d\Omega \end{aligned} \tag{62}$$

where $\Delta\mathbf{u} = \mathbf{u}^{n+1} - \mathbf{u}^n$. Note that both **A** and **G** matrices have to be computed and stored for each time increment.

Integration by parts of $\mathbf{A}_i$ and $\mathbf{g}_i$ terms in (62) gives

$$\begin{aligned}\int_\Omega \mathbf{N}^T \Delta\mathbf{u} d\Omega = -\Delta t \int_\Omega \left[\mathbf{N}^T + \frac{\Delta t}{2}\frac{\partial \mathbf{N}_i^T}{\partial \mathbf{x}_i}\mathbf{A}_i^n\right]\frac{\partial \mathbf{f}_k^n}{\partial \mathbf{x}_k} d\Omega - \\ - \Delta t \int_\Omega \left[\frac{\partial \mathbf{N}_i^T}{\partial \mathbf{x}_j}\mathbf{g}_j + \frac{\Delta t}{2}\left(\mathbf{N}^T\mathbf{G}\frac{\partial \mathbf{f}_i}{\partial \mathbf{x}_i}\right)\right]^n d\Omega + \\ + \oint_\Gamma \left[\frac{\Delta t}{2}\mathbf{N}^T\mathbf{A}_i\frac{\partial \mathbf{f}_k}{\partial \mathbf{x}_k}n_k + \Delta t \mathbf{N}^T\mathbf{g}_k n_k\right]^n d\Gamma\end{aligned} \tag{63}$$

Substituting of (53) into (63) leads to the system of equations

$$\mathbf{M}\Delta\mathbf{a}^n = RHS^n \tag{64}$$

where the right hand side terms RHS can be deduced from (63).

Eq.(64) can be solved using a single or two-step approaches [24,25]. Also if only steady state solutions are to be obtained a lumped mass matrix can be used.

5. ERROR ESTIMATOR AND MESH ADAPTIVITY

For creeping incompressible flow problems the following error norm based on the analogy of Stokes flow with elasticity can be successfully used [32]

$$\|e\|^2 = \int_\Omega ([\dot{\boldsymbol{\varepsilon}} - \hat{\dot{\boldsymbol{\varepsilon}}}]^T[\boldsymbol{\sigma}' - \hat{\boldsymbol{\sigma}}'] - [p - \hat{p}][\dot{\varepsilon}_{ii} - \hat{\dot{\varepsilon}}_{ii}])d\Omega \tag{65}$$

where $\dot{\boldsymbol{\varepsilon}}$, $\boldsymbol{\sigma}'$ and p are exact values of stresses rates, deviatoric strains and pressure and $\hat{(\cdot)}$ stands for computed values.

Since $\dot{\boldsymbol{\varepsilon}}$, $\boldsymbol{\sigma}'$ and p are not known, an approximation of higher order accuracy than that given by the finite element method is used as

$$\|e\|^2 = \int_\Omega ([\dot{\boldsymbol{\varepsilon}}^* - \hat{\dot{\boldsymbol{\varepsilon}}}]^T[\boldsymbol{\sigma}'^* - \hat{\boldsymbol{\sigma}}'] - [p^* - \hat{p}][\dot{\varepsilon}^*_{ii} - \hat{\dot{\varepsilon}}_{ii}])d\Omega \tag{66}$$

Values of $\dot{\boldsymbol{\varepsilon}}^*$ and $\boldsymbol{\sigma}'^*$ can be obtained by projecting the discontinuos numerical solution into a continuos basis. The simplest option is to use nodal averaging of discontinuos element values. However, more sophisticated local and global smoothing techniques can be used [37]. For values of p^* identical procedures can be used. However if p is continuous it is usual to neglected its contribution in the error norm [37].

The porcentage error in the mesh is now defined as

$$\eta = \frac{\|e\|}{\|u\|} \simeq \frac{\|e\|}{\|\hat{u}\|} \times 100 \tag{67}$$

$$\text{with} \qquad \|\hat{u}\|^2 = \int_\Omega (\hat{\hat{\boldsymbol{\varepsilon}}}^T \hat{\boldsymbol{\sigma}}' - \hat{p}\hat{\hat{\varepsilon}}_{ii}) d\Omega \tag{68}$$

The optimal mesh is usually defined as such in which the error is the same for every element. This allows to define the permissible error per element as

$$e_p = \bar{\eta} \left[\frac{\|u\|^2}{n_e} \right]^{1/2} \simeq \bar{\eta} \left[\frac{\|\hat{u}\|^2}{n_e} \right]^{1/2} \tag{69}$$

where $\bar{\eta}$ is a specifed percentage error and n_e is the total number of elements in the current mesh.

The refinement strategy implies the following steps

1) Compute e_p by eq.(69).
2) Compute an error index for each element as

$$\xi^{(e)} = \frac{\|e\|^{(e)}}{e_p} \tag{70}$$

where $\|e\|^{(e)}$ is obtained from eq.(66).

3) Since the error norm is $0(h^m)$ asymptotically where h is the element size and m the order of polynomial in the finite element or finite volume approximations, the new element size is computed as

$$(h^{(e)})_{new} = \frac{[h^{(e)}]_{old}}{[\xi^{(e)}]^{1/m}} \tag{71}$$

In practice the upper and lower limits of $h^{(e)}$ are specifed so that the range of element sizes is controlled.

Examples of applications of this technique for transient and steady state incompressible flow can be found in [32].

For high speed flow situations the error norm (65) can also be used, however the flow-elasticity analogy does not hold and (65) will yield only an approximation of the actual error messure, however useful for practical applications.

A common option in practice for one-dimensional compressible flow problems, is to assume the error for each variable v as

$$e_v \simeq C(h^{(e)})^2 \left| \frac{d^2 v}{dx^2} \right|_e \tag{72}$$

where $|\cdot|_e$ means an average value over the element. The condition of uniform error distribution implies now simply

$$(h^{(e)})^2 \left| \frac{d^2 v}{dx^2} \right|_e = k \text{ (constant)} \tag{73}$$

where $h^{(e)}$ is the element lenght.

Above concepts can be extended to 2D/3D flow situations as follows:

At each element center the following matrix is computed

$$M_{ij}^{(e)} = \frac{\partial^2 v}{\partial x_i \partial x_j} \qquad i,j = \begin{matrix} 1,2 \text{ for 2D problems} \\ 1,2,3 \text{ for 3D problems} \end{matrix} \tag{74}$$

where v is the variable which error is to be computed. Typically $v = \rho$ or $v = M$ (mach number) are chosen.

The eigenvalues of $\mathbf{M}^{(e)}$ are computed (i.e. $\lambda_1^{(e)}$, $\lambda_2^{(p)}$ for 2D problems). From eq.(73) it can be written

$$[h_1^{(e)}]^2 \lambda_1^{(e)} = [h_2^{(e)}]^2 \lambda_2^{(e)} = (h_{min})^2 \lambda_{max} \tag{75}$$

where h_{min} and λ_{max} are the specified values of the minimum element size and the maximum eigenvalue computed in the mesh, respectively.

Eq.(75) yields the new element sizes as

$$h_i^{(e)} = h_{min} \sqrt{\frac{\lambda_{max}}{\lambda_i}} \qquad i = 1,2 \text{ for 2D} \tag{76}$$

Usually $h_1^{(e)} = h_2^{(e)}$ is taken, thus implying equal size elements. However the possibility of stretching the elements (i.e. $h_1^{(e)} \neq h_2^{(e)}$) has also been successfully exploited in practice [22,23].

The mesh is redefined using the new element sizes given by (76). This can imply either refinement or enlargement of some element zones. The definition of the new mesh can be based on the enrichment of the previous one, subdividing or eliminating elements, or in the complete regeneration of a new mesh [19,20,22–25]. For the second option an efficient mesh generator for triangular or quadrilateral elements of different orders has to be used. This mesh generator developed at CIMNE allows to combine structured with unstructured meshes in the same domain. An example of application is the modelling of the boundary layer region with an structured mesh whereas an unstructured mesh is used for the rest of the flow domain (see Examples 6.2.5 and 6.2.6). The unstructured mesh generator developed and used in the examples presented nextis based on the advancing front technique [22], [24].

6. EXAMPLES

6.1 Numerical examples of incompressible flow problems

In this section we present two examples solved using the SUPG penalty formulation described in Sections 2.4–2.6. It is not our aim to give a complete description of the following tests, but rather to show that the method developed is robust an efficient. We recall that the basic ideas are the use of the SUPG formulation to deal with the convective term, a mixed velocity–pressure interpolation leading to div–stable elements and the elimination of the (already interpolated) pressure through penalization. Results obtained compare very well with those reported in the literature.

6.1.1 *Flow over a forward step*

Figures 6a and 6b show the domain and the pressure contours obtained. The domain has been descretized using a uniform structured mesh with 1721 nodal points and 408 biquadratic elements and linear interpolation for the pressure within each element (see Figure 1). In the left boundary (inflow) a parabolic velocity profile has been prescribed. The Reynolds number based on the maximum value of this profile and the step height is 167. The boundary on the right has been left free and zero velocities has been prescribed every where die.

A detail of the streamlines in the recirculation zone is shown in Figure 6c. The position of the reattachment point agrees with other results found in the literature using finer meshes.

6.1.2 *Flow past a cylinder*

The streamlines pattern and the domain are shown in Figure 7. A uniform velocity has been prescribed on the left boundary and zero normal velocities on the upper and lower boundaries, whereas the right one has been left free. The Reynolds number based on the cylinder diameter is 100. The domain has been discretized using 500 biquadratic elements with linear interpolation for the pressures (Figure 1), giving a total of 2100 nodal points.

The symmetric steady–state solution perturbed by a rotating velocity field near the cylinder has been used as initial condition to advance in time. We have used the Crank–Nicolson scheme (backward Euler for the first time step) with a time increment $\Delta t = 0.3$ and Newton–Raphson iterations within each time step.

Results shown in Figure 7b correspond to time step *No.* 301, when the oscillations in the velocity field behind the cylinder are fully developed. The period of these oscillation has been found to be 6 time units.

(a)

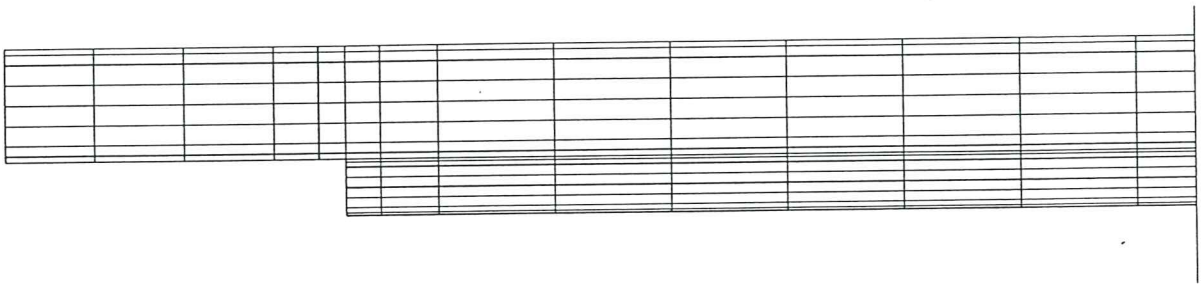

(b)

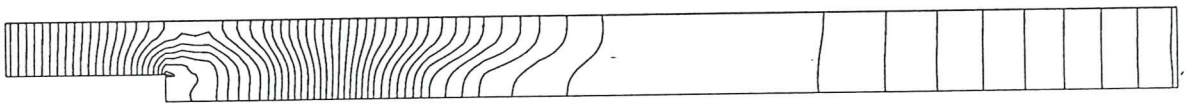

$max = 0.165\ ,\quad min = 0.038$

(c)

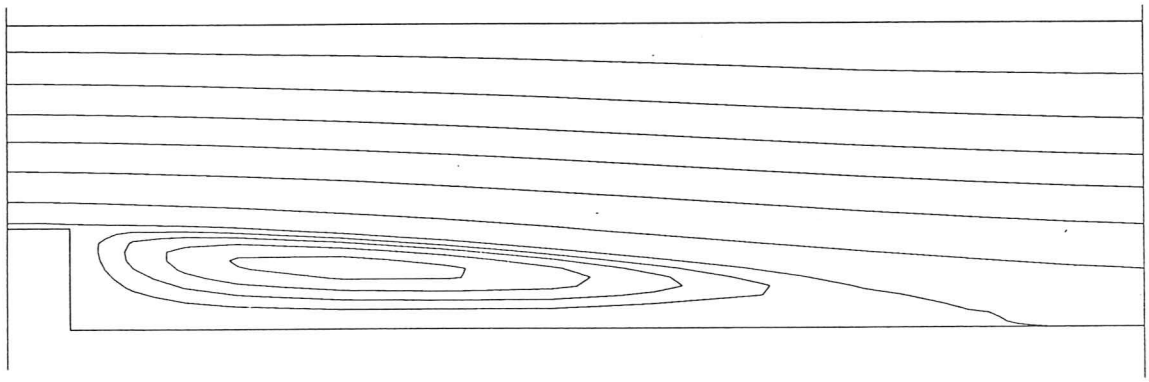

Figure 6 Viscous flow over a forward step ($Re = 500/3$). (a) Geometry and FE mesh of 408 biquadratic elements with linear pressure interpolation. (b) Pressure contours. (c) Streamlines in the circulation zone.

(a)

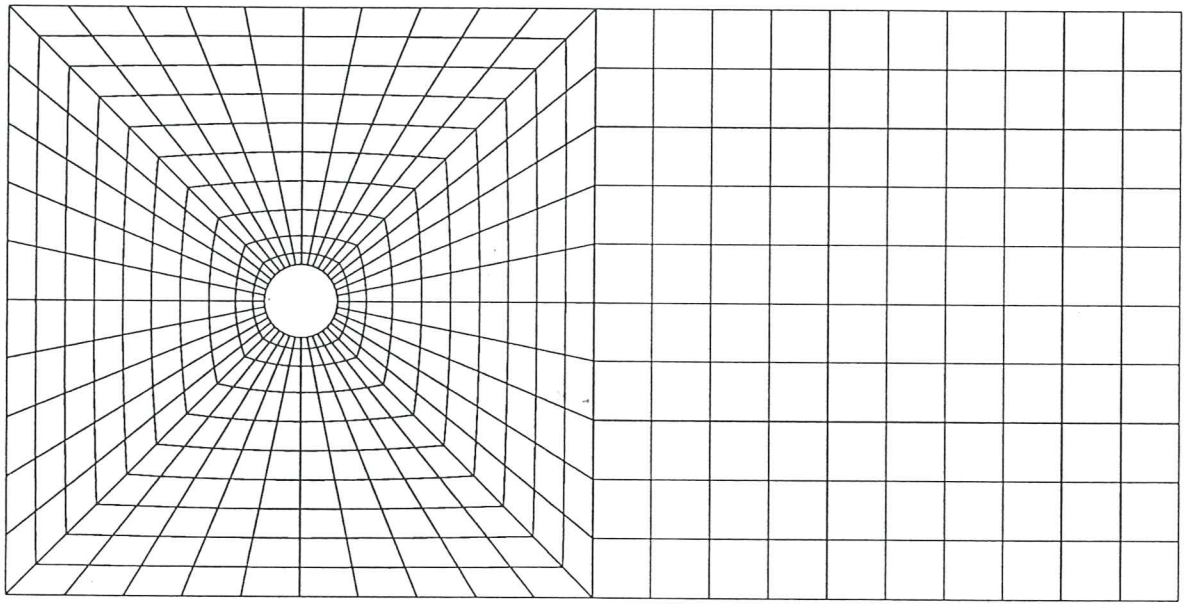

(b)

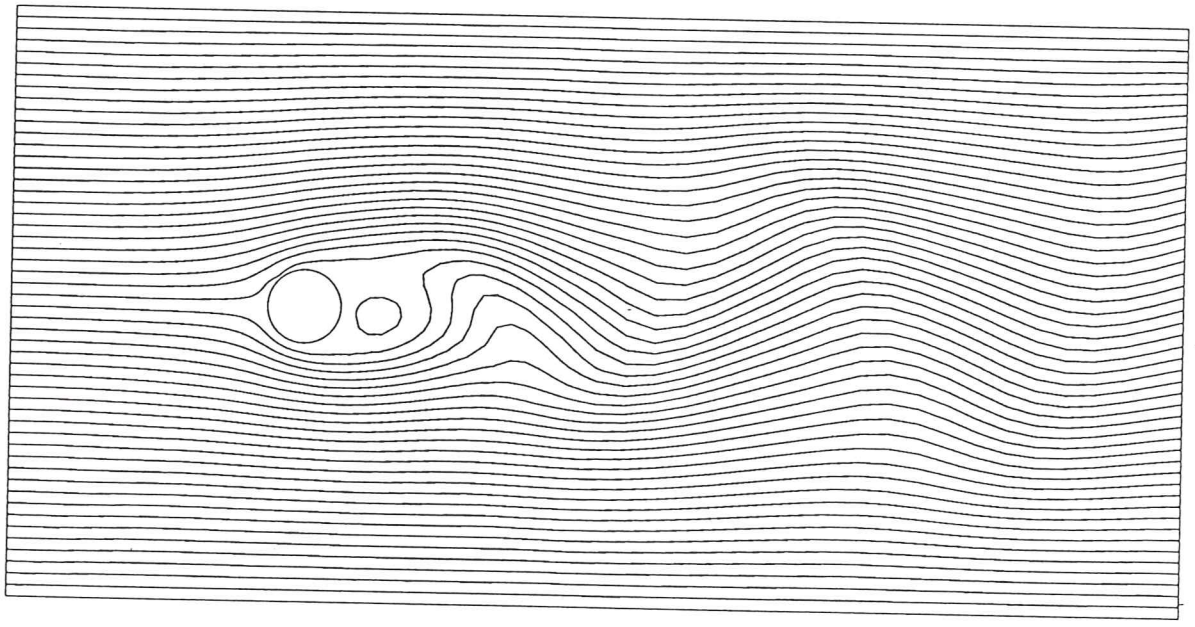

Figure 7 Flow past a cylinder. (a) Geometry and mesh of biquadratic elements with linear interpolation for pressure. (b) Streamlines pattern for time step 301 ($\Delta t = 0.3$).

6.2 Examples of high speed compressible flow

6.2.1 *Mach 5 inviscid flow over a compression corner*

Figure 8 shows the geometry of the problem and the initial mesh of 250 three node triangular elements with equal interpolation for all variables. The analysis has been performed using the Taylor-Galerkin approach presented in Section 4.4. Figure 8 also shows the sequence of adaptive remeshings and the results for the pressure contours obtained with each mesh. The improvement in the definition of the shock is obvious.

6.2.2 *Mach 5 inviscid flow with compression and expansion*

The compression ramp geometry of the previous example was extended to include an expansion corner. Numerical results for this problem were obtained with the Petrov-Galerkin approach proposed in Section 4.3 using again linear triangles. The initial and improved meshes and the pressure contours are shown in Figure 9.

6.2.3 *Mach 3 inviscid flow over a wedge*

The Taylor-Galerkin approach is now applied to the analysis of a high speed inviscid flow over a wedge. The initial and final meshes of linear triangles together with the corresponding Mach number contours are shown in Figure 10. Again the improvement in the solution by the adaptive procedure is substantial.

6.2.4 *Hypersonic inviscid flow over a double ellipse*

This example corresponds to the laminar inviscid non reactive flow past a double ellipse for $M_\infty = 8.5$ and $\alpha = 30°$. The temperature at infinity is $56° K$ and at the body $288°$ K. Again numerical results have been obtained with a Taylor-Galerkin approach and 3 node equal interpolation triangles. Figure 11 shows the finite element meshes obtained after three consecutive remeshings together with the Mach number and the pressure contours for the final mesh. The plots of the pressure coefficient and the Mach number variation along the stagnation streamline also the finer mesh are also shown in Figure 11 [20].

6.2.5 *Hypersonic viscous flow past a double ellipse*

This case is an extension of previous example to viscous flow conditions. A value of $Re = 1.67 \times 10^7$ has been assumed. The full Taylor-Galerkin aproach for viscous flows presented in Section 4.5 has been used.

Figure 12a shows the final finite element mesh of 3 remeshings of 16212 elements and 8315 nodes. Note that the boundary layer region has been modelled using an structured mesh of linear triangles whereas an structured mesh is used in the rest of the flow domain. Details of the boundary layer

discretization and the Mach number contours are shown in Figures 12b and 12c, respectively.

Separated flow conditions in the upper fuselage region obtained in this case as deduced from the final contours of specific total energy are shown in Figure 13a. A study of convergence has also been performed. Figure 13b shows contours of residuals at the first time increments showing high errors in the boundary layer region as expected.

A small global time step has been used during the first 300 time increments to prevent instabilities during the build–up of the boundary layer. A plot of the residual contours in the converged steady state regime is shown in Figure 13c, where the separation effect can clearly be observed.

Figure 14a shows the variation of the specific total energy along the stagnation streamline. The step gradients of the shock and the boundary layer are captured without oscillations. The same effect is observed in the variation of the Mach number along some directions across the shock plotted in Figure 14b.

Finally, Figure 15 shows the paths of some flow particles and details of the recirculating flow near the canopy. For further details on this example see [25'].

6.2.6 *Hypersonic viscous flow past a 2D ramp*

The flow conditions are the following $M_\infty = 10$, $Re = 143800$, temperature at infinity $50°K$ and at the wall $290°$ K.

Figure 16a shows the final finite element mesh of 11440 elements and 5914 nodes. Again a structured mesh was used to model the boundary layer zone, whereas an unstructured mesh was used in the rest of the flow region.

In this case due to the low Reynols number a thick boundary layer appears and no recirculations was observed (see Figure 16b). The Mach number and density contours are shown in Figures 16c and 16d, respectively where the shock induced by the boundary layer build up is clearly detected [25'].

7. CONCLUSIONS

In this work a detailed study of the solution of incompressible and compressible flows using finite elements has been performed.

The use of a SUPG penalty formulation together with compatible velocity–pressure approximations provides a robust computational framework for the solution of incompressible viscous flow problems.

For compressible flows accurate oscillation–free solutions have been obtained with the Taylor–Galerkin approach for both insviscid and viscous flow problems using simple linear triangular elements. This is in line with recent research reported on the ability of the Taylor–Galerkin approach to overcome the div–stability LBB conditions [36].

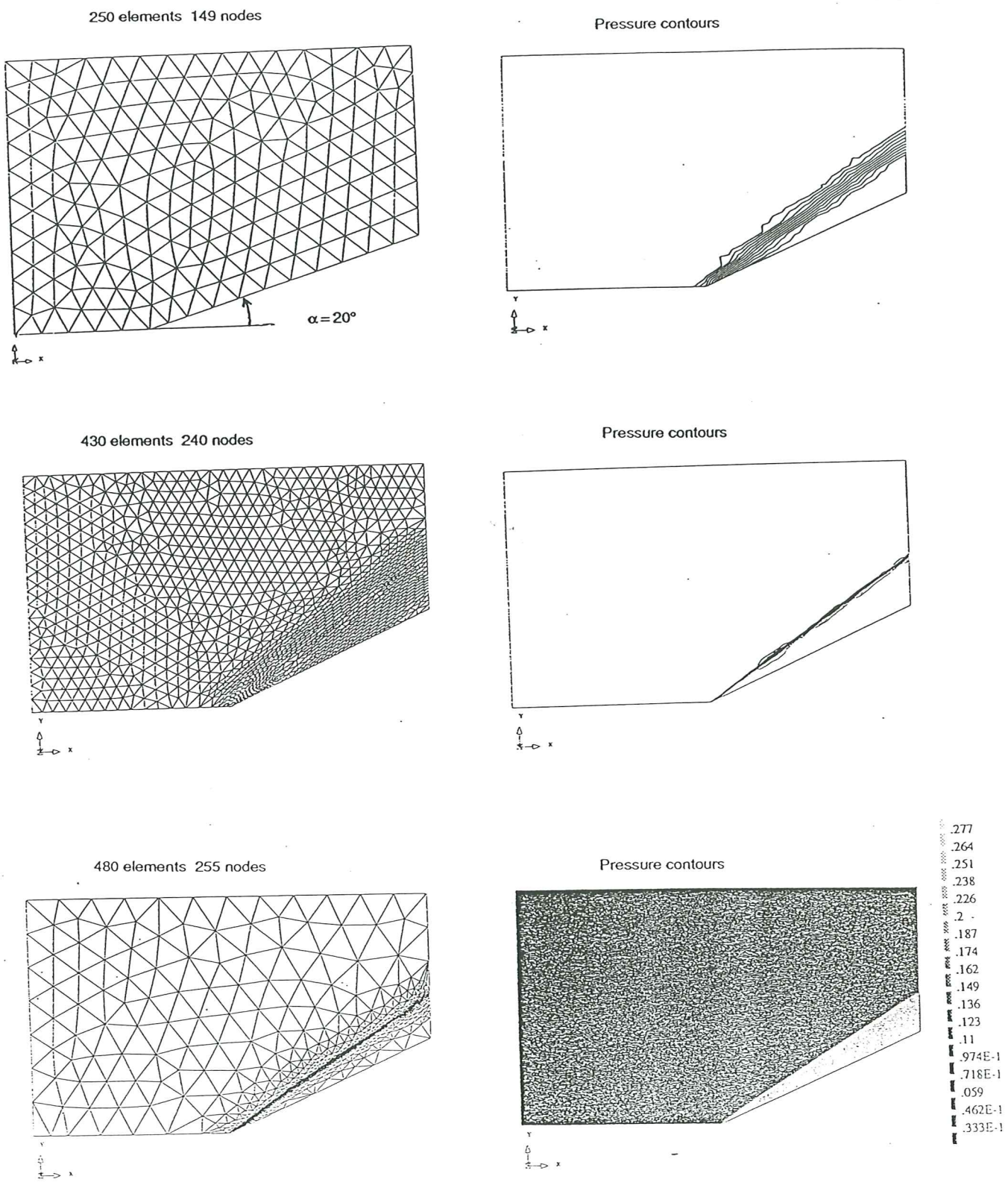

Figure 8 Mach 5 invisid flow over a compression corner. Sequence of refined meshes of linear triangular elements and pressure contours.

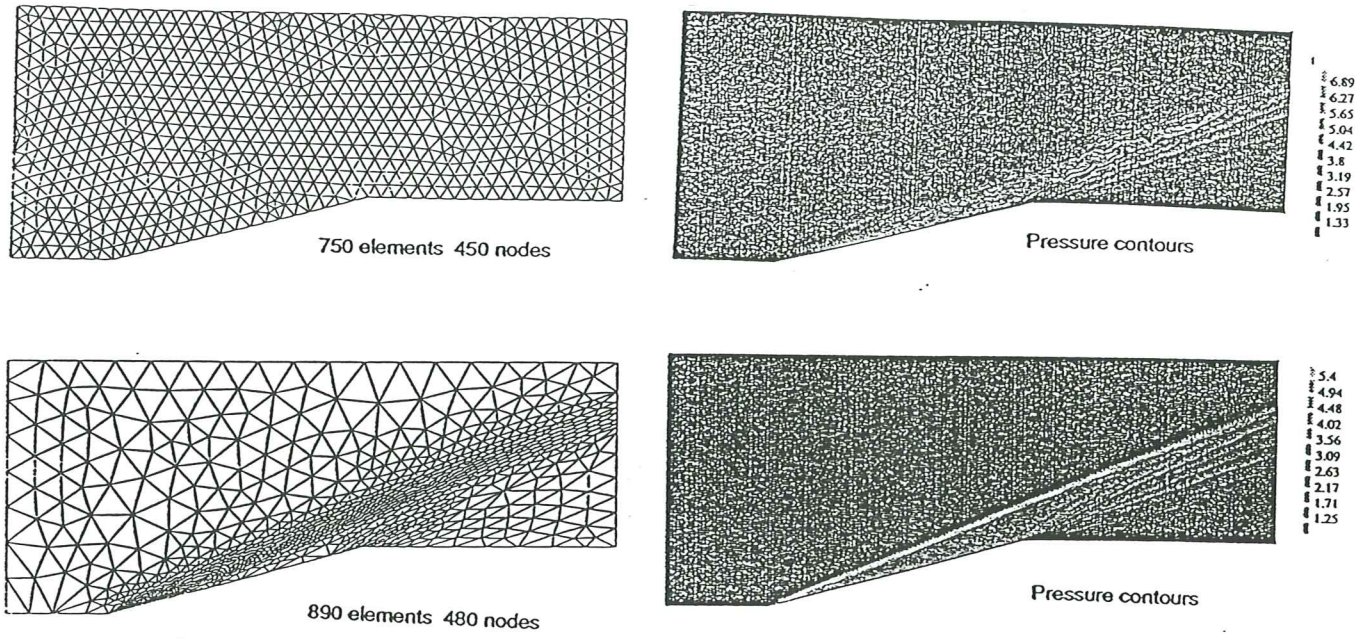

Figure 9 Mach 5 inviscid flow with compression and expansion. Initial and refined meshes of linear triangular elements and pressure contours.

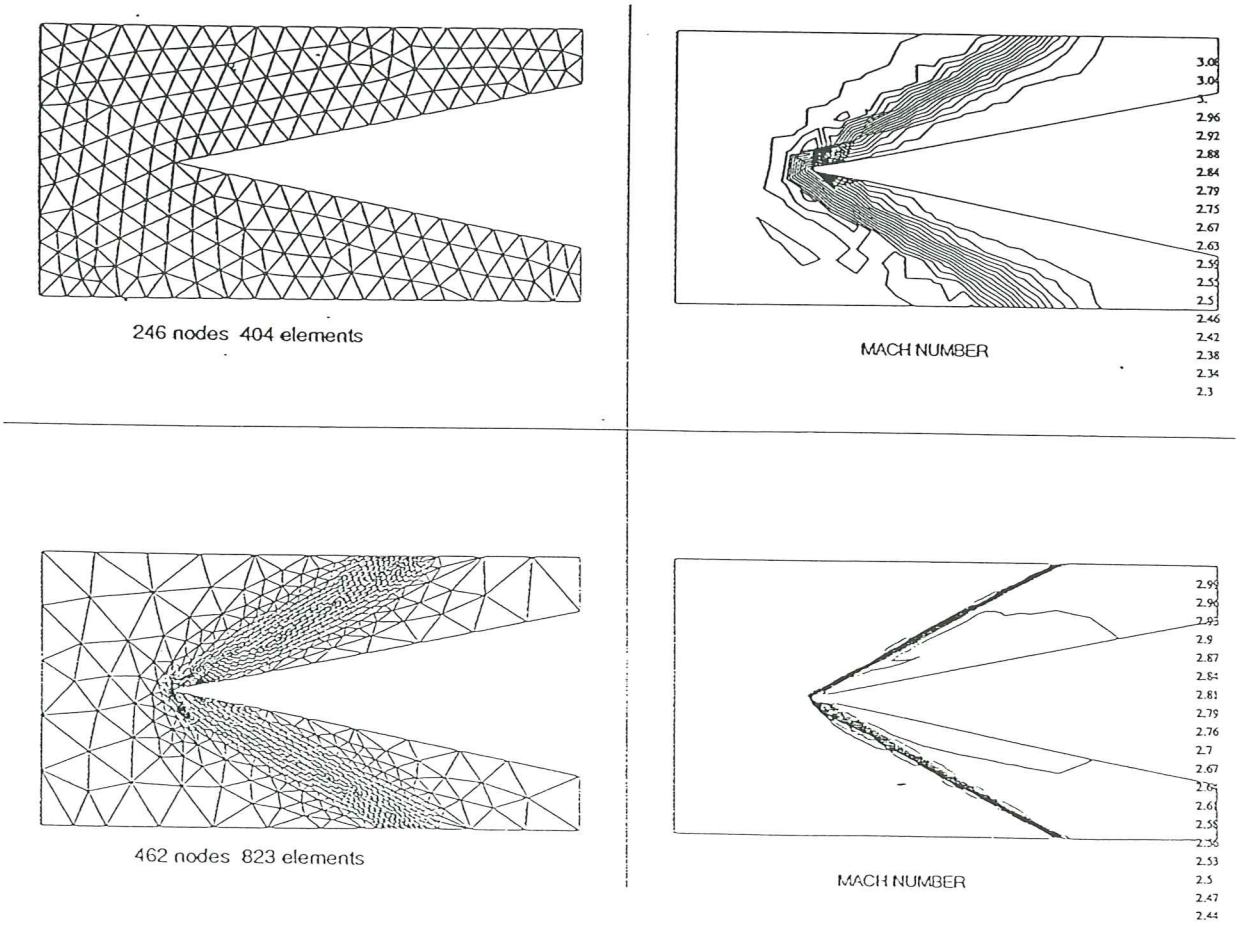

Figure 10 Mach 3 inviscid flow over a wedge. Initial and refined meshes of linear triangles and Mach number contours.

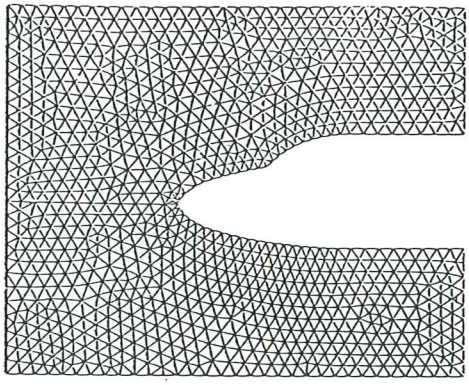

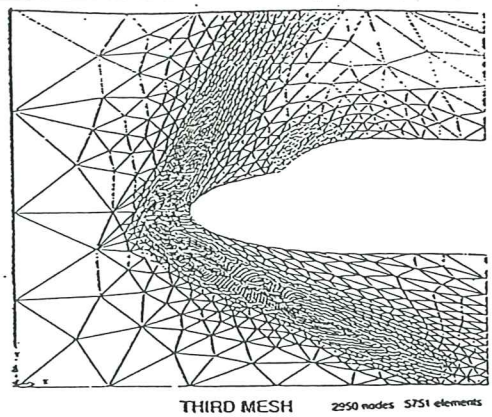

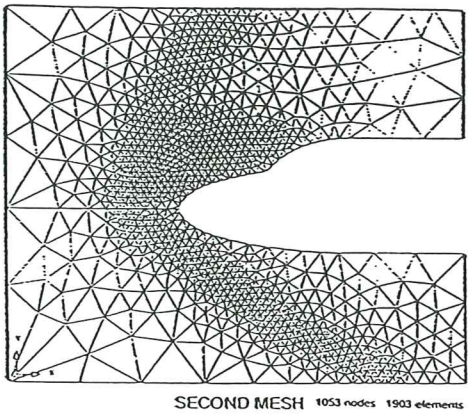

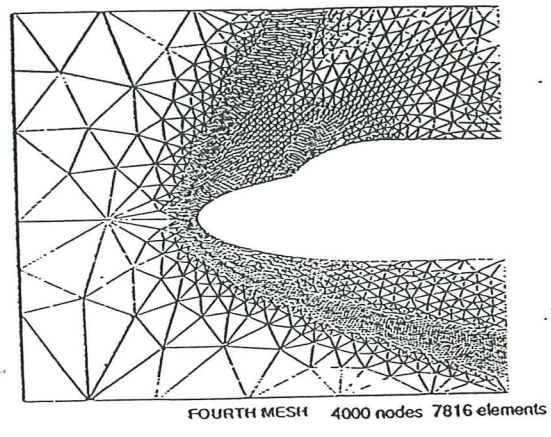

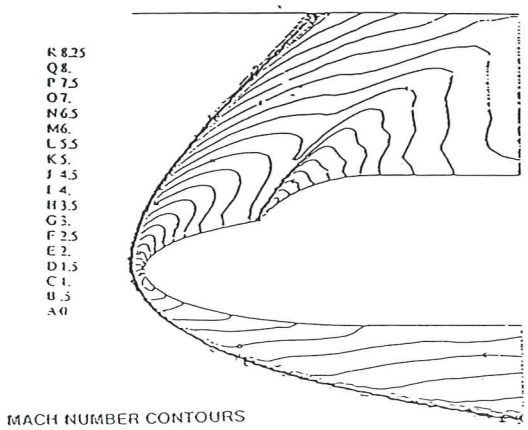

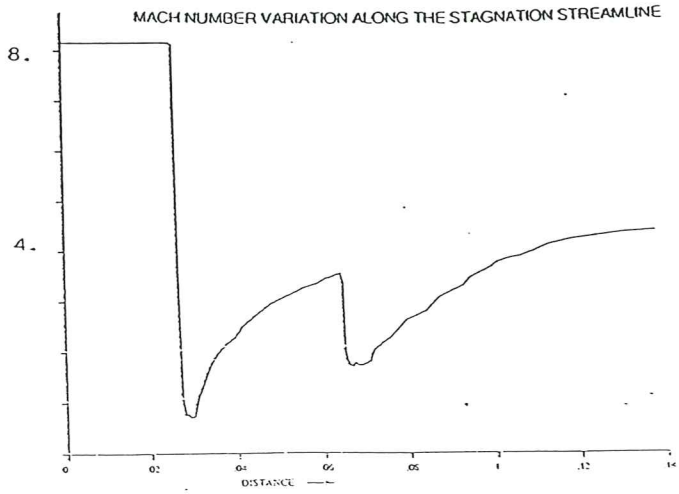

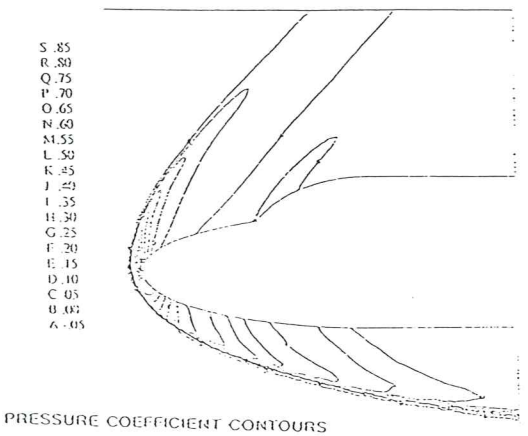

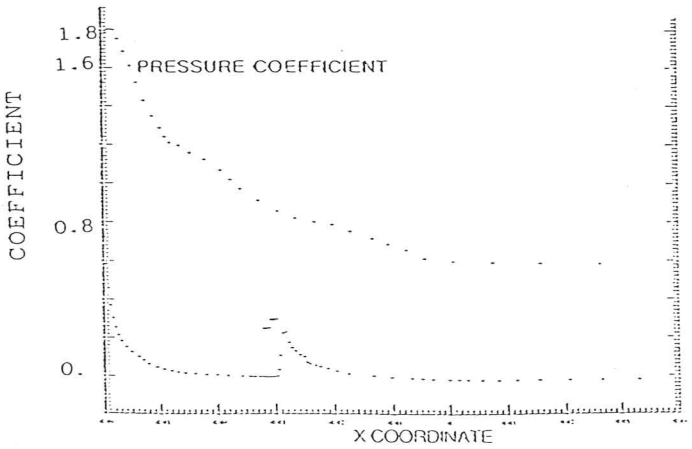

Figure 11 Hipersonic inviscid flow ($M_\infty = 8.5, \alpha = 30^o$) over a double ellipse. Sequence of refined meshes. Mach number and pressure contours and plots of pressure coefficient and Mach number variation for the finer mesh.

(a)

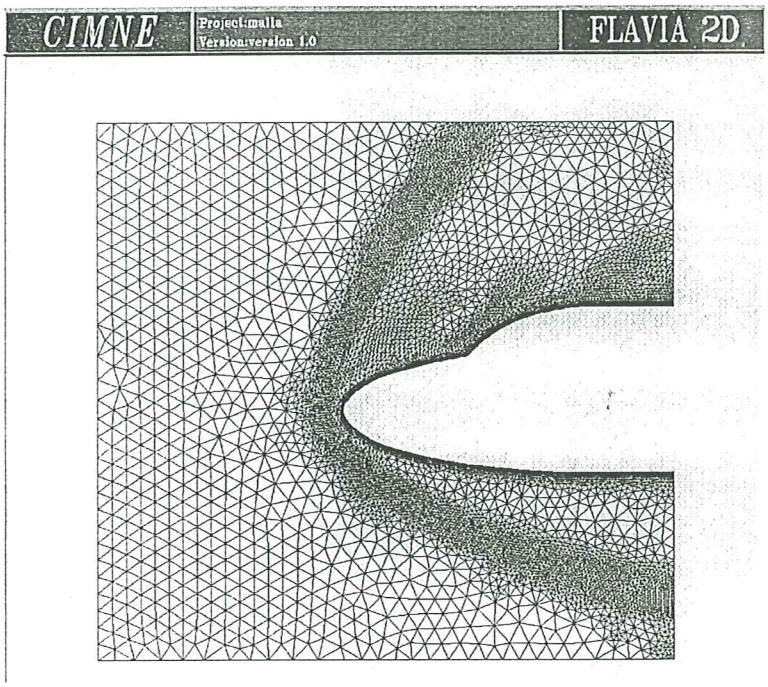

(b)

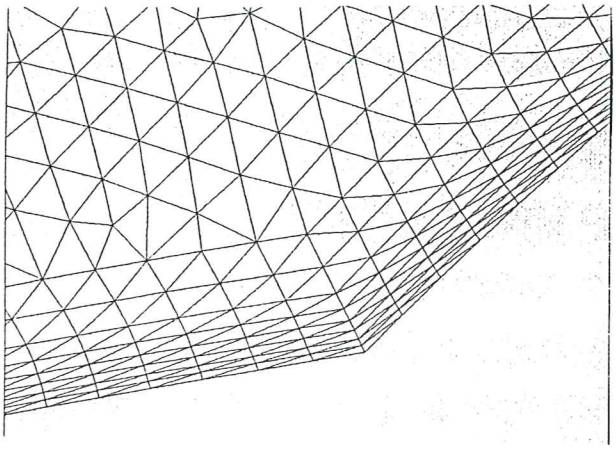

(c)

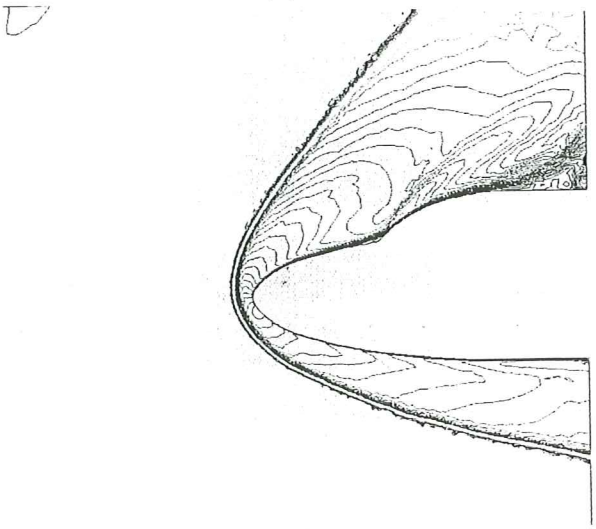

Figure 12 Hypersonic viscous flow ($M_\infty = 8.5$) past a double ellipse. (a) Mesh of 16212 linear triangular elements. (b) Detail of structured meshing in boundary layer region. (c) Mach number

(a)

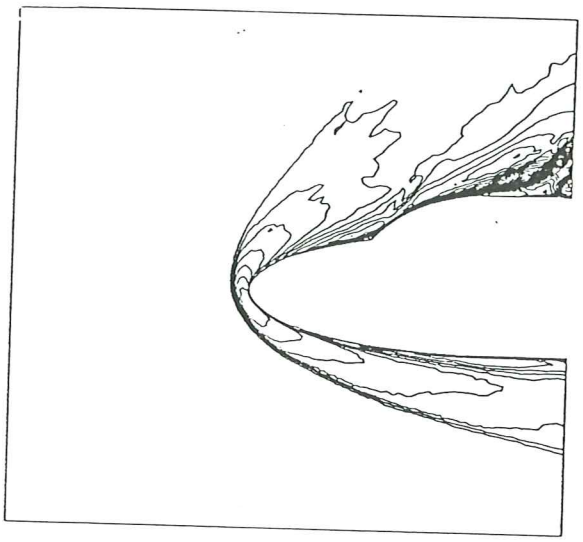

(b)

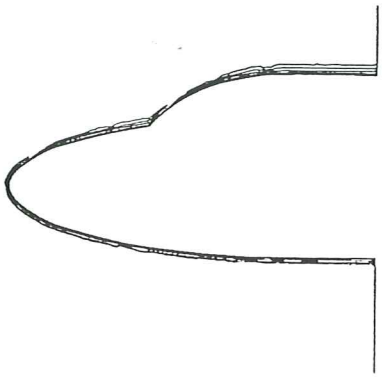

(c)

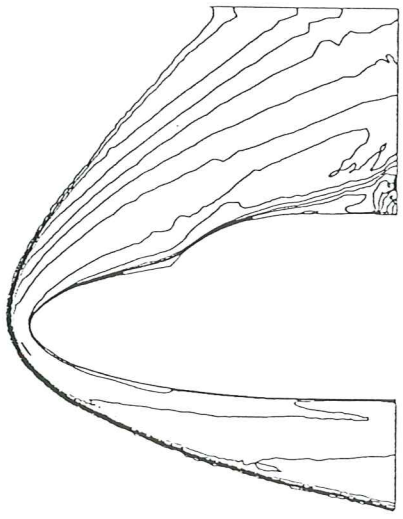

Figure 13 Hypersonic viscous flow ($M_\infty = 8.15$) past a double ellipse. (a) Final contours of specific energy. (b) Contours of residuals errors at onset of iterations. (c) Contours of residual error at final solutions.

(a)

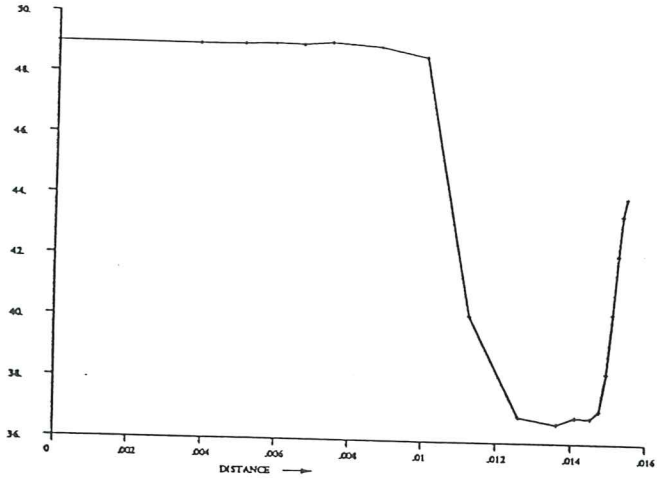

(b)

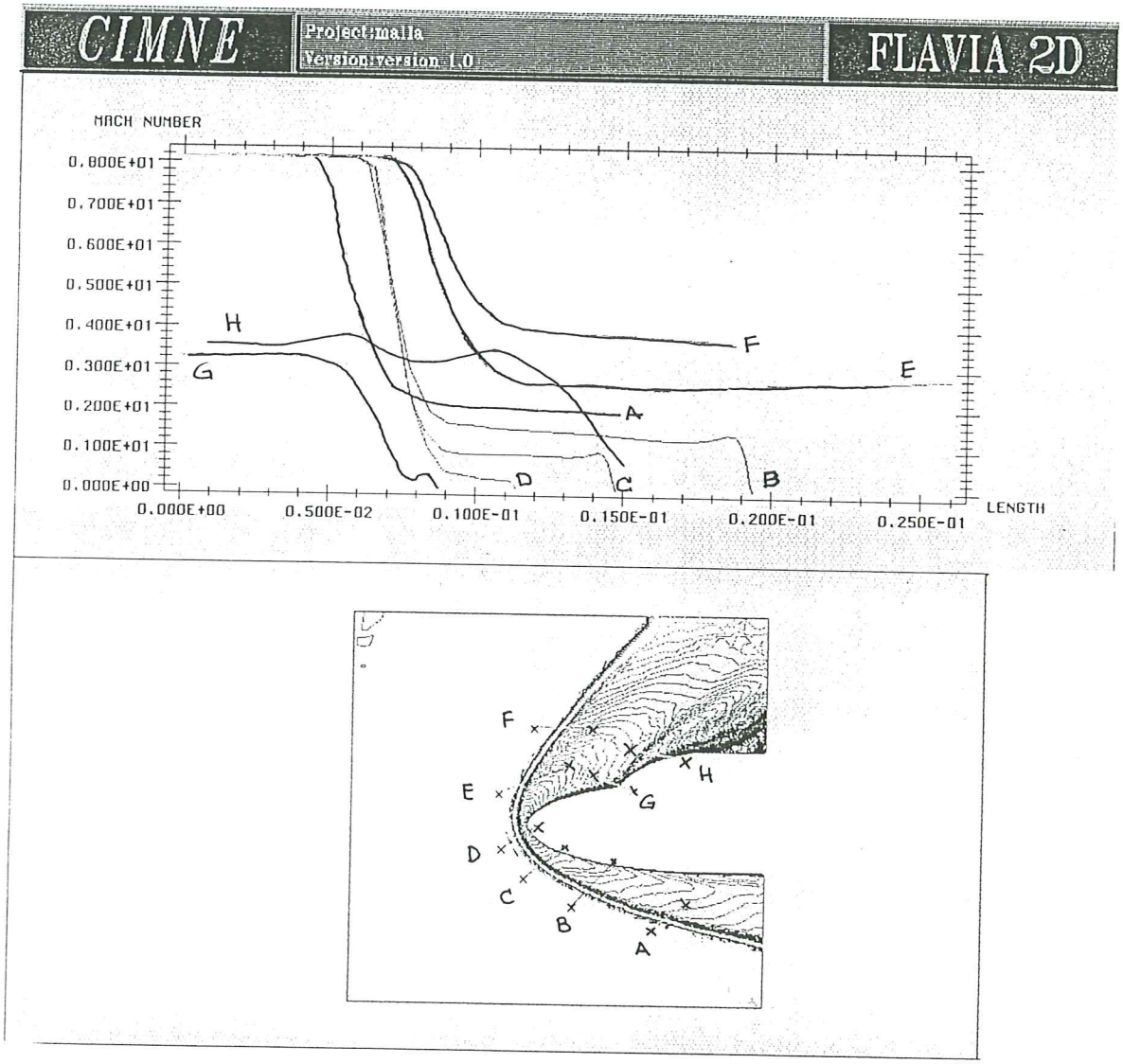

Figure 14 Hypersonic viscous flow ($M_\infty = 8.15$) past a double ellipse. (a) Variation of total specific energy along the stagnation streamline. (b) Variations of Mach number along some selected directions.

(a)

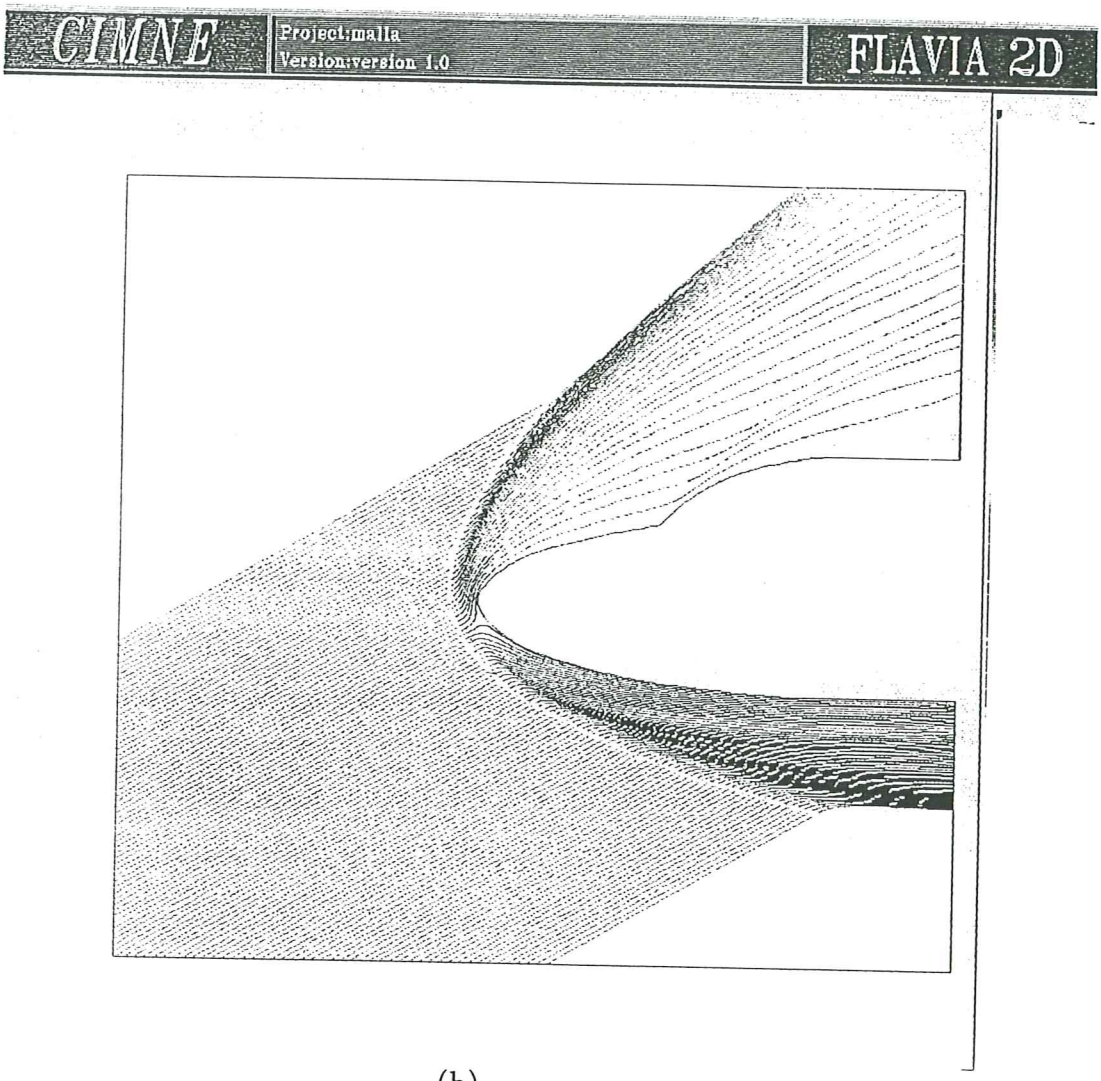

(b)

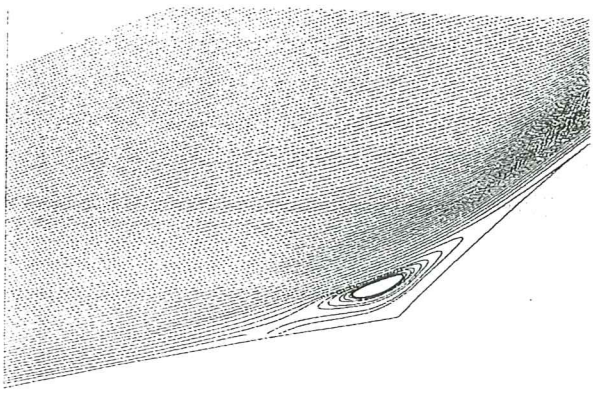

Figure 15 Hypersonic viscous flow ($M_\infty = 8.15$) past a double ellipse. (a) Paths of some flow particles. (b) Recirculating flow near the canopy.

(a)

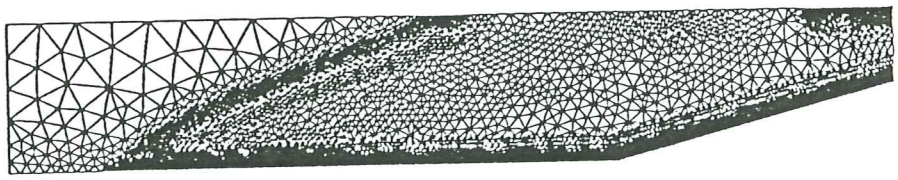

(b)

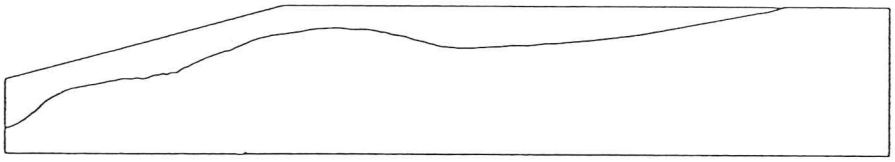

(c)

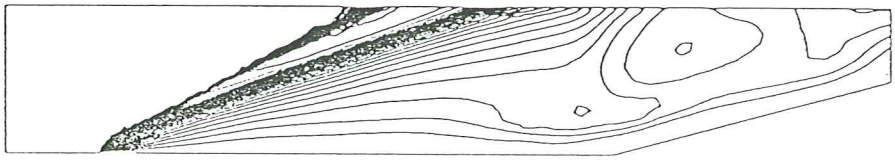

(d)

Figure 16 Hypersonic viscous flow ($M_\infty = 10$) past a 2D ramp. (a) Mesh of 11440 linear triangular elements. (b) Approximated thickness of boundary layer. (c) Mach number contours. (d) Density contours.

Further research at CIMNE in these areas will address topics such as the development of robust finite element algorithms for the solution of coupled thermal–flows in the incompressibility range, the assesment of the robustness of the Taylor–Galerkin approach in combination with compatible elements, the definition of the optimal mesh for each particular problem and the study of the general cost-efficiency of the computational models developed.

ACKNOWLEDGEMENTS

The authors thank Dr. M. Cervera for his essential help in the development at CIMNE of program FANTOM used for the analysis of examples of Section 6.1. The contribution of Mr. U. Shaeffer in the development of FANTOM is also gratefully acnowledged. Thanks are given to Dr. G. Bugeda who provided the visualizationl program FLAVIA and the adaptive mesh generator both developed at CIMNE, with which examples of Sections 6.2 were analyzed. Dr. J. Peiró an Prof. J Peraire are thanked for his useful comments and for providing original software for mesh generation and analysis of compressible flow. Finally, the authors thank Profs. O.C. Zienkiewicz and J. Periaux for many fruitful discussions.

REFERENCES

1. Bernardi, C., Bristeau, M.O., Periaux, J., Pironeau, O. and Vallet, M.G., "Numerical analysis for compressible viscous isothermal stationary flows", *ASME Workshop*, Minneapolis, 1990.
2. Brezzi and F., Douglas, J., "Stabilized mixed methods for the Stokes problem", *Num. Math.,*, vol. **53**, pp. 129–151, 1988.

2'. A.N. Brooks, T.J.R. Hughes, " streamline Upwind/Petrov–Galerkin formulations for convective dominated flows with particular emphasis on the incompressible Navier–Stokes equations", *Comp. Meth in Appl. Mech. and Engng.*, vol. **32**, pp. 199–259, 1982.

3. Brueckner, F. and Heinrich, J.C., "Petrov-Galerkin finite element model for compressible flow". To be published in *Int. J. Num. Meth. Engng.*

3'. Brueckner, F., "Finite element analysis of high speed flows with application to the ram accelerator concept", Ph.D. Thesis, University of Arizona, 1991

4. Christie I. and Mitchell, A.R., "Upwinding of high order Galerkin methods in condution-convection problems", *Int. J. Num. Meth. Engng.*, vol. **14** , pp. 1764–1771, 1978
5. Codina, R., Oñate, E. and Cervera, M., "The intrinsic time for the SUPG formulation using quadratic elements", Submitted to *Comp. Meth. Appl. Mech. Engng.*, 1990
6. Donea, J., "A Taylor-Galerkin method for convective transport problems", *Int. J. Num. Meth. Engng.*, vol. **20**, pp. 101–119, 1984

7. Fortin, M. and Glowinski, R., "*Methodes de Lagrangien Augmente*", Dunod, Paris, 1982
8. Galeao, A.C., Dutra do Carmo, E.G., "A consistent approximate upwind Petrov-Galerkin method for convection-dominated problems", *Comp. Meth. in Appl. Mech. and Engng.*, vol. **68**, pp. 83–95, 1988
8'. P.M. Gresho, S.T. Chan, R.L. Lee, C.D. Upson, "A modified finite element method for solving the time–dependent incompressible Navier–Stokes equations"Part I: Theory, *Int. J. Num. Met. in Fluids*, vol. 4, pp. 557–598, 1984.
9. Hassan, O., Morgan, K. and Peraire, J., "An adaptive implicit/explicit finite element scheme for compressible viscous high speed flows". *AIAA*, 27th Aerospace Sciences Meeting, Reno, Nevada, January, 1989
10. Heinrich, J.C. and Zienkiewicz, O.C., "The finite element method and upwinding techniques in the numerical solution of convection dominated flow problems", in *Finite Element Methods for Convection Dominated Flows*, T.J.R. Hughes (ed.) 1979
11. Hirsch, C., "*Numerical computation of internal and external flow*", vol. **I**, J. Wiley, 1989
12. Hughes T.J.R. and Brooks, A.N., "A theoretical framework for Petrov-Galerkin methods, with discontinuous weighting functions: Applications to the streamline upwind procedure", in *Finite elements in fluids*, R.H. Gallagher, D.M. Norrie, J.T. Oden and O.C. Zienkiewicz (eds.), vol. **IV**, pp. 46–65, Wiley, London, 1982
13. Hughes, T.J.R., Franca, L.P. and Hulbert, G.M., "A new finite element formulation for computational fluid dynamics: VIII. The Galerkin/least-squares method for advective-diffusive equations", *Comp. Meth. in Appl. Mech. and Engng.*, vol. **73**, pp. 173–189, 1989
14. Hughes, T.J.R., Franca, L.P. and Balestra, M., "A new finite element formulation for computational fluid dynamics: V. Circumventing the Babuška-Brezzi condition: A stable Petrov-Galerkin formulation for the Stokes problem accomodating equal-order interpolations", *Comp. Meth. in Appl. Mech. and Engng.*, vol. **59**, pp. 85–99, 1986
15. Johnson, C., "The Streamline Diffusion finite element method for compressible and incompressible fluid flow", *Von Karmam Lecture Series, IV: Computational Fluid Dynamics*, March 1990
16. Kawahara, M. and Ohmiya, K., "Finite Element Analysis of Density Flow Using the Velocity Correction Method", *Int. J. Num. Meth. Fluids*, vol. **5**, pp. 981–993, 1985
17. MacDonal, P.W., "The computation of transonic flow through two dimensional gas turbine cascades", *ASME*, paper 71-GT-89, 1971
18. MacCornack, R.W. and Paulay, A.J., "Computational efficiency achieved by time splitting of finite difference operators", *AIAA*, paper 72-154, San Diego, 1972

19. Morgan, K., Peraire, J., Thareja, R.R. and Stewart, J.R., "An adaptive finite element scheme for the Euler and Navier-Stokes equations". *AIAA*, 8th CFD conference, Honolulu, Hawai, June, 1987
20. Oñate, E., Quintana, F. and Miquel J., "Numerical simulation of hypersonic flow over a double ellipse using a Taylor Galerkin finite element formulation with adaptive grids". Proceedings of the workshop an Hypersonic Flows for Reentry Problems, Antibes, January 1990, Periaux, J. and Desideri, M. (Eds.), INRIA, 1991

20'. Oñate, E., Codina, R., Quintana, F. and Miquel, J., "Report on the reseach developed up to November 30th 1990 in HERMES contract ANE 1/88 step 2.", *Informe CIMNE*, IT-25, December 1990

21. Patankar, S.V., "*Numerical heat transfer and fluid flow*", Hemisphere Publishing Corp., 1980
22. Peiro, J., "*A Finite Element Procedure for the Solution of the Euler Equations on Unstructured Meshes*". PhD Thesis, University of Wales, Swansea, 1989
23. Peraire, J., "*A finite element method ofr convection dominated flows*", PhD Thesis, University of Wales, Swansea, 1986
24. Peraire, J., Vahdati, M., Morgan, K. and Zienkiewicz, O.C., "Adaptive remeshing for compressible flow computations", *J. Comp. Physics*, vol. **72**, pp. 449–486, 1987
25. Peraire, J., Peiro, J., Formaggia, L., Morgan, K. and Zienkiewicz, O.C., "Finite element Euler computations in three dimensions", *Int. J. Num. Meth. Engng.*, vol. **26**, pp. 2135–59, 1988

25'. Quintana, F., Oñate, E. and Miquel Canet, J., "Flow and temperature computations for space vehicles using adaptive finite elment techniques", Presented at the First European Symposium on Aerothermodynamics for Space Vehicles, ESA–ESTEC, Noordwijk, 28–30, May 1991.

26. Rizzi, A.W. and Inouye, M., "Time split finite volume methods for three dimensional blunt body flows", *AIAA Journal*, pp. 1478–85, 1973
27. Sampaio, P.A.B., "A Petrov-Galerkin formulation for the incompressible Navier-Stokes equations using equal order interpolation for velocity and pressure", to appear in *Int. Num. Meth. Engng.*, 1990
28. Schneider, G.E., Raithby, G.D. and Yovanovich, M.M., "Finite element analysis of incompressible fluid flow incorporating equal order pressure and velocity interpolation", in *Numerical Methods in Laminar and Turbulent flow*, C. Taylor, K. Morgan, C.A. Brebbia (Eds.), Pentech Press, Plymouth, 1978
29. Sohn, J.L. and Heinrich, J.C., "A Poisson equation formulation for pressure calculation in penalty finite element models for viscous incompressible flows", *Int. J. Num. Meth. Engng.*, vol. **30**, pp. 344–71, 1990
30. Taylor, R.L. and Zienkiewicz, O.C., "Mixed finite element solution of fluid flow problems" in R.H. Gallagher et al. (Eds.), *Finite Element in Fluids*, vol. **4**, J. Wiley, 1982
31. Taylor, R.L., Zienkiewicz, O.C., Simo, J.C. and Chan A.H.C., "The Patch Test

– A condition for asessing FEM convergence", *Int. J. Num. Meth. Engng.*, vol. **22**, pp. 39–62, 1986

32. Wu, J., Zhu, J.Z., Smelter, J. and Zienkiewicz, O.C., "Error estimation and adaptivity in Navier-Stokes incompressible flow", *Computational Mechanics*, vol. **6**, 4, pp. 259–71, 1990
33. Zienkiewicz, O.C., Jain, P.C. and Oñate E., "Flow of solids during forming and extrussion. Some aspects of numerical solution", *Int. J. Solids, Struct.*, vol. **14**, 15–38, 1978
34. Zienkiewicz, O.C., Heinrich, J.C. and Oñate E., "General formulation for coupled thermal flow of metals using finite elements", *Int. J. Num. Meth. Engng.*, vol. **17**, pp. 1497–514, 1981
35. Zienkiewicz, O.C., Qu, S., Taylor, R.L. and Nakazawa, S., "The Patch Test for mixed formulations", *Int. J. Num. Meth. Engng.*, vol. **23**, pp. 1873–1883, 1986
36. Zienkiewicz, O.C. and Wu, J., "Incompressible without tears. How to avoid restrictions of mixed formulations", Internal report, University College of Swansea, U.K., 1990
37. Zienkiewicz, O.C. and Taylor, R.L., "The finite element method", Mc Graw Hill, vol. **I**, 1989, vol. **II**, 1991
38. Zienkiewicz, O.C. and Oñate E., "Finite volumes vs. finite elements. Is there really a choice?", in *Non linear Computational Mechanics. State fo the Art.*, P. Wriggers and W. Wagner (Eds.), Springer-Verlag, 1991